Transient CB2 receptor activation triggers irreversible luminal differentiation via chromatin remodeling in breast cancer

Nuria G. Martínez-Illescas[1,2], Gemma Pérez-García[1], María Rubert-Hernández[2,3], Camila Quezada-Gutiérrez[1], Estrella Martín-Zapater[1], Luis M. Alonso-Colmenar[4], Carmen Hernández[4], Ángela Zarco-Cuadrillero[5], Eduardo Caleiras[6], Miguel Muñoz-Ruiz[5], Ana Payo-Payo[7], Laura Frías-Aldeguer[8], Cristina Sánchez[2,3], Mercedes Balcells-Camps[9,10], Elazer R. Edelman[9], María Salazar-Roa[1,2]*

1 Cancer STEM Lab, Dept. Biochemistry and Molecular Biology, Faculty of Biological Sciences, Complutense University (UCM), Madrid, Spain

2 Breast and Gynecologic Cancer Group, Research Institute i+12; Madrid, Spain

3 Dept. Biochemistry and Molecular Biology, Faculty of Biological Sciences, UCM, Madrid, Spain

4 Flow Cytometry and Fluorescence Microscopy Unit, UCM, Madrid, Spain

5 Dept. Immunology, Faculty of Medicine, UCM, Madrid, Spain

6 Histopathology Unit, Spanish National Cancer Research Center, Madrid, Spain

7 Animal Ecology Lab, Dept. Biodiversity, Ecology and Evolution, Faculty of Biological Sciences, UCM, Spain

8 Mammary Pathology Unit, Hospital La Paz, Madrid, Spain

9 Harvard-MiT Biomedical Engineering Center, MIT Institute for Medical Engineering and Science, Cambridge, US

10 Instituto Químico de Sarriá (IQS), School of Engineering, Ramon Llull University, Barcelona, Spain

**Correspondence should be addressed to María Salazar-Roa (mariasalazarroa@ucm.es)*

Abstract

Cellular plasticity enables cancer cells to escape therapy by adopting stem-like or alternate lineage states. Here, we identify a mechanism by which cannabinoid receptor 2 (CB2R) activation promotes irreversible lineage commitment in breast cancer. Using patient-derived and murine organoids, we show that brief, low-dose exposure to CB2R agonists—either phytogenic or synthetic—induces a basal-to-luminal transition, accompanied by reduced self-renewal, invasiveness, and tumor-initiating potential. These changes are retained under conditions that normally promote dedifferentiation, including fibroblast co-culture, immune pressure, and mechanical shear stress.

Mechanistically, CB2R engagement initiates a transient chromatin remodeling program, marked by early expression of pluripotency-associated genes followed by silencing and differentiation commitment. This epigenetically stabilized state renders tumor cells more responsive to tamoxifen and limits the emergence of resistant clones.

Our findings uncover a previously unrecognized role for CB2R in modulating cancer cell identity and suggest new opportunities to constrain tumor plasticity by directing differentiation through a drug-responsive pathway.

42 **Introduction**

43 Recent evidence of cellular plasticity and spontaneous de-differentiation suggests that
44 cancer developmental landscape is far more complex than a simple hierarchical structure.
45 "Phenotypic plasticity," a newly recognized hallmark of cancer, plays a significant role in this
46 complexity (1). Traditional cancer treatments, such as cytotoxic drugs and radiotherapy, primarily
47 aim to target cell division through mechanisms of widespread cell damage and toxicity. However,
48 these approaches often prove inefficient and may create evolutionary pressures that favor the
49 emergence of aggressive, resistant cancer clones. In some cases, cytotoxic treatments even
50 promote undesirable side effects, such as metastasis.

51 In contrast, differentiation therapies aim to induce terminal differentiation in cancer cells,
52 effectively removing them from the proliferative compartment (2, 3). By promoting differentiation
53 in a subset of tumor cells, these therapies can alter tumor dynamics by limiting the growth
54 potential of the entire tumor. This effect is akin to habitat fragmentation, where differentiated cells
55 occupy space and resources that would otherwise be used for tumor expansion, thereby
56 restricting the carrying capacity. Notably, when differentiation strategies are combined with
57 cytotoxic therapies, tumor dynamics can shift from growth to regression (3).

58 Tumors with high stem cell traits are, therefore, ideal candidates for differentiation-based
59 and potentially, combined therapies. The mammary gland, a tissue characterized by significant
60 postnatal development and cyclical expansion, exhibits considerable stem cell plasticity. This
61 plasticity is particularly relevant in the context of poorly differentiated breast carcinomas, which
62 are known for their rapid spread and high incidence of metastasis, making them a major challenge
63 in cancer treatment. Indeed, a significant proportion of breast cancer-related deaths are attributed
64 to relapse or dissemination after surgery/therapy, a phenomenon most commonly observed in
65 patients with poorly differentiated tumors (4). While the direct relationship between tissue
66 differentiation and partial pathologic complete response (pCR) after treatments remains unclear
67 (5, 6), existing correlations emphasize the need of differentiation-based treatment approaches.

68 Designing effective differentiation therapies requires an understanding of the parallels
69 between cancer and embryonic development. Many signalling pathways involved in
70 embryogenesis are aberrantly reactivated in cancer, with genetic and epigenetic changes driving
71 this process (7-11). These pathways, including Wnt/β-catenin (12), Hedgehog (Hh) (13), Notch

72 (14), TGF-β (15), PI3K /AKT (16) and JAK/STAT (17), govern cellular differentiation during normal
73 development. In cancer, their reactivation contributes to disease pathology, driving the
74 reprogramming of tumor cells to a progenitor-like state—a key feature of metastasis. Notably, the
75 endocannabinoid system (ECS) has been shown to regulate many of these pathways (18).

76 The ECS is a complex cellular network that regulates a variety of physiological functions
77 (19, 20). It consists of two main cannabinoid receptors, CB1R and CB2R, their endogenous
78 ligands (AEA and 2-AG), and associated proteins responsible for their synthesis, transport, and
79 degradation. Over the past two decades, substantial evidence has demonstrated that ECS
80 activation has anti-tumor effects in cell and animal models, including promoting tumor cell death,
81 inhibiting endothelial cell migration, blocking tumor angiogenesis, and suppressing tumor cell
82 adhesion and migration (21, 22). Much of this research has focused on cannabinoids derived
83 from *Cannabis sativa*, which contains over 500 compounds, including the primary cannabinoids
84 Δ9-tetrahydrocannabinol (THC) and cannabidiol (CBD) (23). Additionally, synthetic cannabinoid
85 receptor ligands have shown similar effects in cancer models (24). These findings have prompted
86 clinical trials investigating the safety and efficacy of cannabinoids as anti-tumor agents (25-28).

87 In this study, we expand the therapeutic potential of cannabinoids by exploring their use
88 as differentiation drivers in cancer. Using three-dimensional organoids derived from breast cancer
89 mouse models and patient biopsies, we demonstrate that both natural and synthetic Cannabinoid
90 Receptor 2 (CB2R) ligands promote long-term and stable tumor cell differentiation when
91 administered at low doses (nanomolar concentrations) and short treatment regimens (4 days
92 followed by drug withdrawal). Moreover, combining these differentiation strategies with
93 tamoxifen—a widely used breast cancer treatment—significantly enhances therapeutic outcomes
94 while allowing for reduced chemotherapy doses and exposure, thus mitigating undesirable side
95 effects.

96 **Results**

97 **Low-dose, transient THC exposure durably reprograms mammary tumor organoids,**
98 **disrupting cancer cell plasticity *in vitro* and *in vivo*.**

99 Cannabinoids have been widely studied for their anti-tumor properties—suppressing
100 proliferation, invasion, metastasis, and promoting autophagy and cell death [recently reviewed in
101 (18)]. However, their role in regulating tumor differentiation remains poorly understood. Since
102 differentiation therapies align with adaptive treatment strategies aimed at reducing tumor
103 evolution and resistance (29), we first examined whether low-dose THC could durably modulate
104 tumor cell plasticity.

105 To test this, we exposed MMTV-PyMT mammary tumor organoids to nanomolar vs.
106 micromolar concentrations of THC. While high doses triggered expected cytotoxic effects, 10 nM
107 THC induced significant long-term morphological and molecular changes exclusively in 3D
108 cultures, but not in 2D (**Supp. Fig. 1**). Based on this, we developed a protocol using a 4-day 10
109 nM THC pulse, followed by extended drug-free culture (**Fig. 1A**). Strikingly, this short, low-dose
110 exposure consistently induced a basal-to-luminal switch, both morphologically (**Fig. 1B–E**) and
111 at the molecular level (**Fig. 1F–G**), highlighting a stable reprogramming effect on tumor cell
112 identity. These effects were replicated in organoids derived from MMTV-Her2/neu tumors (**Supp.**
113 **Fig. 2**), confirming that THC-driven differentiation is not model-specific. Functionally, THC
114 treatment inhibited collective migration, triggered a mesenchymal-to-epithelial transition (MET)
115 (**Fig. 2A–D**), and reduced stem-like features and self-renewal capacity (**Fig. 2E–G**). These
116 phenotypes were also validated in patient-derived breast cancer organoids (**Supp. Fig. 3**),
117 underscoring their potential clinical relevance.

118 To assess functional *in vivo* consequences, THC-treated and control organoids were
119 orthotopically injected into wild-type PyMT mice (**Fig. 3A–B**). THC-pretreated organoids showed
120 markedly reduced tumor initiation capacity, and the few tumors that did form exhibited delayed
121 growth and non-malignant histology, in contrast to controls which developed aggressive
122 neoplasias (**Fig. 3C–E**). In tail-vein injection assays, THC-pretreated organoids produced
123 significantly fewer lung micro- and macro-metastases compared to controls (**Fig. 3F–I**).

124 Together, these findings reveal that brief, low-dose THC exposure durably reprograms
125 tumor cell fate, reducing plasticity, stemness, and metastatic potential both *in vitro* and *in vivo*.

126 **CB2 receptor mediates cannabinoid-induced differentiation in breast cancer organoids.**

127 To explore the role of cannabinoid receptor tone in tumor cell differentiation, we
128 compared the effects of pure phytocannabinoids (THC, CBD), *Cannabis sativa* extracts, and
129 methanandamide (mAEA)—a metabolically stable analog of the endocannabinoid AEA—on
130 MMTV-PyMT-derived mammary tumor organoids. As shown in **Supplementary Fig. 4**, both
131 extracts and pure cannabinoids induced similar morphological changes, reduced collective
132 migration, and promoted a basal-to-luminal molecular switch. In contrast, mAEA did not equally
133 influence differentiation, maybe due to its low affinity for CB2R. We next assessed synthetic
134 inverse agonists of cannabinoid receptors: SR1 (CB1R) and SR2 (CB2R). Interestingly, SR2, but
135 not SR1, recapitulated THC effects—inducing durable basal-to-luminal reprogramming, inhibiting
136 migration (**Fig. 4A–E**), and reducing self-renewal (**Fig. 4F**). This unexpected finding suggested a
137 functional role for CB2R in regulating tumor plasticity. Combining THC with either SR1 or SR2 did
138 not block its long-term effects on morphology, migration, or organoid size (**Supp. Fig. 5A–D**),
139 implying that CB2R modulation is sufficient but not necessarily required for THC-mediated
140 reprogramming. Supporting this, CB2R expression modestly increased following cannabinoid
141 treatment in differentiation-responsive contexts (**Supp. Fig. 5E**).

142 To directly test the role of CB2R, we generated CB2R knockout mice (MMTV-PyMT
143 CB2R^{-}/$^{-}$). These mice developed tumors with delayed onset compared to wild-type controls
144 (**Supp. Fig. 6A**), consistent with previous observations in other models (30). CB2R deficiency
145 also altered tumor biology—lower Ki67 and SOX gene expression suggested reduced
146 proliferation and stemness (**Supp. Fig. 6B**). While flow cytometry revealed no major shifts in
147 EpCAM/CD49f-defined subpopulations between CB2R^{-}/$^{-}$ and WT tumors (**Supp. Fig. 6C**), the
148 capacity to form viable organoids from luminal progenitors was significantly impaired in CB2R^{-}/$^{-}$
149 mice (**Supp. Fig. 6D**). Additionally, CB2R knockout organoids exhibited distinct basal-like
150 morphologies, reduced size, diminished collective migration, and decreased long-term self-
151 renewal (**Supp. Fig. 6E–J**), closely resembling the phenotype induced by THC and SR2.

152 Together, these findings identify CB2R signaling as a key modulator of tumor
153 differentiation, capable of driving durable reprogramming in breast cancer organoids.

154

THC and SR2 trigger an early, transient epigenetic reprogramming in breast cancer organoids, driving sustained cellular differentiation.

Cellular differentiation is tightly linked to epigenetic remodeling, yet the connection between CB2R signaling and epigenetic regulation in cancer remains poorly defined (18). To investigate this relationship, we conducted transcriptomic profiling of mammary tumor organoids treated with THC or SR2, focusing on genes related to epigenetic control and stemness. As shown in **Figure 5**, both treatments triggered a distinct, phase-specific gene expression program. By day 3, organoids displayed a transcriptional signature enriched for embryonic and pluripotency-associated genes (**Fig. 5A–D**), reminiscent of the early reprogramming stages observed in ESCs and iPSCs. This transient increase in plasticity was followed by a clear shift toward a differentiation-related transcriptional profile at later time points (**Fig. 5E**), underscoring a structured reprogramming process.

Gene set enrichment and differential expression analyses revealed broad modulation of epigenetic regulators involved in histone modifications, chromatin remodeling, and DNA methylation (**Fig. 5C**). These changes aligned with increased accessibility at bivalent chromatin domains (**Fig. 5D, 5F, 5G**), suggesting that CB2R signaling may facilitate transcriptional priming and epigenetic poising of differentiation programs. Indeed, among the top transiently expressed genes, Utf1 emerged as particularly notable—a key regulator of Polycomb Repressive Complex (PRC) activity and pluripotency maintenance (31, 32). Utf1 was upregulated early after THC or SR2 exposure, and subsequently downregulated at later stages, reflecting the transition from a plastic to a more differentiated state (**Fig. 5B**). Consistent with this, the expression of *bona-fide* UTF1 and PRC2 target genes was synchronously modulated under our experimental conditions (**Fig. 5F–G**). Furthermore, we confirmed bivalent histone marks in organoids treated with THC and SR2, which indeed induced a balanced ratio of H3K27me3/ H3K4me3, reinforcing the role of bivalent chromatin regulation in establishing and maintaining cannabinoid-induced differentiation programs (**Fig. 5H–I)**.

Together, these results demonstrate that short-term CB2R activation triggers a transient epigenetic reset, effectively priming mammary tumor organoids for long-term, stable differentiation.

185 **CB2R-driven differentiation locks tumor cells into a stable, irreversible phenotype.**

186 A critical limitation of current differentiation therapies is their potential reversibility,
187 especially under microenvironmental pressures that favor stemness and aggressiveness (2). To
188 challenge the stability of CB2R-induced differentiation, we developed a dynamic co-culture
189 system mimicking a pro-tumorigenic niche. This system included cancer-associated fibroblasts
190 (CAFs), peripheral blood mononuclear cells (PBMCs), and continuous shear stress via a flow-
191 controlled bioreactor (**Fig. 6A and Supp. Fig. 7**). As expected, co-culture with CAFs significantly
192 enhanced tumor cell migration, and reinforced basal and mesenchymal traits in tumor organoids
193 (**Supp. Fig. 7A–E**). These effects, along with a significant increase in organoid size, were further
194 amplified by the inclusion of PBMCs and shear stress (**Supp. Fig. 7F–J**), confirming the model's
195 capacity to promote cellular plasticity and invasive behavior. Remarkably, even under these
196 challenging microenvironmental conditions, both THC and SR2 treatments effectively
197 reprogrammed tumor organoids toward a luminal, differentiated state and maintained this
198 phenotype over time (**Fig. 6B–E**). Notably, this differentiation state persisted despite prolonged
199 exposure to CAFs, PBMCs, and shear stress, highlighting the durability of cannabinoid-induced
200 reprogramming. To note, cytokine profiling revealed that SR2- and THC-treated co-cultures
201 exhibited a broad activation of immune responses and a reduction in chemokines associated with
202 tumor progression (**Fig. 6F**). Furthermore, cannabinoid-treated organoids displayed sustained
203 epigenetic remodeling, as described above, even within this aggressive microenvironment (**Fig.
204 6G–H**).

205 Collectively, these results demonstrate that CB2R modulation triggers a robust,
206 irreversible differentiation program capable of resisting pro-aggressive cues—supporting its
207 potential as a therapeutic strategy to counteract the inherent plasticity of breast cancer cells.

208

209 **CB2R-driven differentiation sensitizes breast cancer cells to endocrine therapy.**

210 Drug-resistant cancer cells often incur a fitness cost—reduced growth, higher metabolic
211 demands, or lower competitiveness. Adaptive therapy exploits this trade-off by maintaining a
212 population of drug-sensitive cells to suppress resistant clones through natural competition, thus
213 delaying resistance and improving long-term outcomes (33). In this framework, differentiation
214 therapies, including CB2R-targeted strategies, may act as adaptive interventions by reducing

215 tumor stemness and plasticity, thereby lowering resistance potential. To explore this therapeutic
216 synergy, we tested CB2R-mediated differentiation followed by tamoxifen, a widely prescribed
217 endocrine therapy for ER^+ breast cancer (34) (**Fig. 7A**). Transcriptomic profiling revealed that
218 both THC and SR2 treatments significantly enhanced estrogen signaling pathways (**Fig. 5E**),
219 providing a rationale for their combination with tamoxifen. Organoids were first exposed to CB2R
220 ligands for 4 days, and ten days after drug withdrawal, treated with sub-micromolar concentrations
221 of tamoxifen for 4 days. This sequential combination therapy led to reduced cell viability (**Fig. 7B**)
222 and G2-M cell cycle arrest (**Fig. 7C**) in cannabinoid-pretreated organoids. After 4 weeks of drug
223 withdrawal, these first observations translated into a more pronounced basal-to-luminal shift (**Fig.**
224 **7D**), smaller organoid size (**Fig. 7E**), impaired collective migration (**Fig. 7F**) and particularly
225 relevant, reduced long-term self-renewal (**Fig. 7G**). Importantly, CB2R-based pretreatment
226 completely abolished the emergence of resistant clones, which were evident in tamoxifen-only
227 cultures (**Fig. 7G**). This demonstrates that cannabinoid-induced differentiation not only sensitizes
228 tumor cells to endocrine therapy but also prevents adaptive resistance.

229 To validate these observations in clinically relevant settings, we tested the combinatory
230 treatment in patient-derived samples. Surgical specimens from two breast tumors were processed
231 for organoid culture, and the efficacy of the SR2–tamoxifen regimen was assessed following the
232 experimental timeline outlined in **Fig. 8A**. Using phase holographic imaging, we analyzed cancer
233 cell movement and dispersal 10 days after CB2R-based differentiation. Cells pretreated with SR2
234 exhibited reduced motility, altered migration directionality, and changes in cell area and shape
235 irregularity, suggesting impaired adaptation for migration (**Fig. 8B–F and Supp. Fig. 8**). At this
236 same time point, SR2 treatment had also enhanced cell–cell adhesion within the 3D organoids,
237 as evidenced by increased E-cadherin and decreased Snail expression (**Fig. 8G**), along with a
238 marked reduction in organoid size (**Fig. 8H**) and diminished collective migration (**Fig. 8I**).
239 Following this, organoid cultures were exposed to 5 μM tamoxifen for 4 days. Notably, the
240 differentiated cellular state induced by SR2 created a highly favorable context for tamoxifen
241 therapy: organoids pretreated with SR2 showed severely impaired self-renewal following
242 tamoxifen exposure, whereas control organoids retained normal self-renewal capacity despite
243 tamoxifen treatment (**Fig. 8J–K**).Together, these results highlight the potential of CB2R

modulation as a priming strategy to enhance the efficacy of standard treatments, aligning with adaptive therapy principles to improve durable cancer control.

Discussion

Cancer cells undergo numerous molecular and behavioral changes that enable them to overcome natural selection barriers, one of the most notable being the loss of differentiation markers and a reprogramming to a de-differentiated state. This reversion to an earlier developmental stage provides the tumor with increased plasticity and self-renewal capacity.

The standard treatment for cancer traditionally relies on cytotoxic drugs and radiotherapy, both of which induce cell damage and death, especially in highly proliferative cells. However, these therapies are often criticized for their side effects and their tendency to trigger evolutionary pressures, leading to the emergence of resistant and aggressive tumor clones. As a result, there is growing interest in integrating additional therapeutic approaches, including personalized medicine and immune-directed therapies, to improve clinical outcomes. Among the most promising alternatives to cytotoxic treatments are differentiation therapies, which, although proposed over 50 years ago (35) are still being explored. The principle behind these therapies is that cancer cells, to expand and maintain plasticity, often block differentiation processes. Differentiation therapy does not aim to induce cell death but instead focuses on inhibiting self-renewal and guiding tumor cells back toward terminal differentiation.

One of the most successful examples of differentiation therapy is the treatment of Acute Promyelocytic Leukaemia (APL), where a combination of cytotoxic therapy and all-trans retinoic acid (RA) has dramatically improved remission rates and survival outcomes (36, 37). Notably, while RA alone induces high differentiation grades, long-term disease remission is not achieved, suggesting that combination therapies yield the best results. In solid tumors, differentiation therapy is still in its early stages but remains a promising second-line option for patients with advanced cancer.

Our study uncovers a previously unrecognized role for the cannabinoid receptor CB2 (CB2R) in driving stable cancer cell differentiation in breast cancer. We show that a brief, low-dose exposure to THC or the CB2R ligand SR2 durably reprograms mammary tumor organoids,

274 triggering a basal-to-luminal switch, reducing stemness, and impairing migration, self-renewal,
275 and metastatic potential—effects that persist *in vitro* and *in vivo*.

276 Over the past decades, substantial preclinical and clinical evidence has demonstrated
277 that the endocannabinoid system (ECS) regulates several physiological functions, including pain
278 perception, motor coordination, and nausea/vomiting (38), common side effects of chemotherapy.
279 Our lab was among the pioneers in documenting the anti-tumor properties of cannabinoids (39),
280 showing their ability to block proliferation, migration, and angiogenesis (22). These findings laid
281 the groundwork for the first phase 1b randomized, placebo-controlled clinical trial assessing the
282 effects of the cannabis-based drug Sativex on tumor progression in patients with recurrent
283 glioblastoma. This trial demonstrated the safety, tolerability, and lack of interaction with
284 temozolomide (the standard treatment), as well as a notable survival benefit at one year (27).
285 With the increasing legalization of cannabis in over 80 countries, there has been a growing
286 interest in its clinical applications, particularly in cancer treatment.

287 Our study contributes to the expanding body of research on cannabinoids in cancer
288 therapy by focusing on a relatively unexplored application: While cannabinoids have been
289 implicated in nearly all cancer hallmarks (40), their role in differentiation has received less
290 attention. Previous studies, particularly in leukaemia, have shown that THC can sensitize cancer
291 cells to chemotherapeutic agents, reducing IC50 values by approximately 50% and enhancing
292 overall therapeutic effects (41). Additionally, Dronabinol, an FDA-approved cannabinoid, has
293 been shown to inhibit differentiation blockage in acute leukaemia cells (42). In myelomas, THC
294 has been found to induce differentiation of myeloid-derived suppressor cells, reducing immune
295 evasion (43). Most studies have used cannabinoid concentrations in the micromolar range (1-25
296 μM) (44, 45), with effects typically observed after prolonged exposure. In contrast, our study is
297 the first to evaluate the anti-cancer effects of cannabinoids at nanomolar concentrations (10 nM)
298 in three-dimensional organoid models derived from both mouse and human solid tumors.
299 Moreover, we assess the long-term impact of a brief cannabinoid exposure (4 days), followed by
300 drug withdrawal for at least two weeks, a novel approach that has not been previously explored.
301 Significantly, this work also shows that, after cannabinoid treatment, tumors can be subjected to
302 chemotherapy at reduced doses, resulting in improved therapeutic outcomes. Therefore, our data

303 illustrate a new potential practice of adaptive therapy, with important implications in tumor cell
304 plasticity and relapse impairment.

305 Intriguingly, we found that THC, SR2, and CB2 receptor knockout (CB_2KO) cells exhibit
306 similar effects on cancer cell differentiation. Although THC is known to be a partial agonist at both
307 CB1 and CB2 receptors (46) and SR2 is an inverse agonist of CB2R, THC may act also as an
308 inverse agonist at CB2 receptors in a stemness context, or its brief and low-dose exposure might
309 stimulate a CB2-CB1 receptor switch, similar to what has been observed in neuronal
310 differentiation (47-49). This hypothesis aligns with the idea that CB2 receptors are overexpressed
311 in cancer, contributing to tumor aggressiveness, and that cancer differentiation would involve the
312 downregulation of CB2 receptors and a (potential) subsequent upregulation of CB1 receptors
313 (50). Those exciting possibilities are out of the scope of this work but deserve broader research.

314 Our work shows that brief exposure to CB2R ligands such as THC or SR2 significantly
315 enhances the long-term differentiation potential of cancer cells, even after multiple passages,
316 suggesting an epigenetic mechanism. In fact, RNAseq analyses revealed and early remodeling
317 of the epigenetic landscape, apparently establishing a form of replication memory, that promoted
318 a sustained differentiated state several weeks after treatment. Among the top genes regulated by
319 THC or SR2, Undifferentiated Transcription Factor 1 (UTF1) likely plays an important role in this
320 effect. Extensive research supports its function as a central mediator of epigenetic stability, both
321 in early embryogenesis (51), governing lineage specification, and in cancer, when it has been
322 showed to bind chromatin with histone-like dynamics, maintaining nuclear structure during cell
323 fate transitions (31, 52, 53). Mechanistically, UTF1 localizes to promoters of developmental
324 genes—particularly those that are silenced or bivalently marked (e.g., H3K4me3 and H3K27me3),
325 fine tuning the balance between self-renewal and differentiation (32). Indeed, its expression
326 diminishes as cells begin to differentiate. Collectively, these findings position UTF1 potentially
327 explaining the long-term effects of transient CB2R ligand exposure on cancer cell differentiation.

328 Synthetic CB2R ligands have shown great promise in pharmacological research, with
329 conceivable applications in neurodegenerative diseases, autoimmune disorders, chronic pain,
330 and cancer (54). However, clinical testing of CB2R-targeted compounds is still in its early stages.
331 Our findings provide strong support for the therapeutic potential of SR2 as differentiation agent in
332 cancer, since our data show that SR2-treated organoids exhibit even stronger differentiation

333 effects than those treated with THC. These results, combined with recent advances in CB2R
334 pharmacology, suggest a promising future for CB2R synthetic ligands in novel cancer therapy.
335
336 **Methods**
337
338 ***Animal models and procedures***
339 All animal procedures were approved by the Animal Experimentation Committee of the
340 Complutense University of Madrid (CEIyBA) and the Regional Government of Madrid, in
341 compliance with European animal research regulations. Mice were housed under a 12-hour
342 light/dark cycle with ad libitum access to food and water. PyMT mice [FVB/N-Tg(MMTV-
343 PyMT)$^{634Mul/J}$] were generously provided by Miguel Quintela (CNIO, Spain). The MMTV-
344 neu:CB2R$^{-/-}$ strain was previously developed in our laboratory (30) and MMTV-neu [FVB/N-
345 Tg(MMTV-neu)$^{202Mul/J}$] mice were obtained by selecting CB2R$^{+/+}$ individuals from this colony. To
346 generate the PyMT:CB2R$^{-/-}$ line, PyMT mice were crossed with MMTV-neu:CB2R$^{-/-}$ mice. The
347 CB2R$^{-/-}$ allele was introduced through four generations of backcrossing, during which the neu
348 transgene was also eliminated. Genotyping was performed using the following primers (5′−3′; F:
349 forward, R: reverse). **PyMT**, F: TGC CGG GAA CGT TTT ATT AG; R: GGA ACA AGT ACC CCA
350 GCT CA; **CB2R-WT/KO**, F: CTA CAA AGC TCT AGT CAC CCG; WT-R: GGC TCC TAG GTG
351 GTT TTC ACA TCA GCC TCT; KO-R: CTA AAG CGC ATG CTC CAG AC; **Neu**, F: GCT CAG
352 AGA CCT GCT TTG GA; R: AGG AGG ACG AGT CCT TGT AGT G. PCR was performed using
353 the following protocol: 95 °C for 15 min; 30 cycles of 94 °C for 30 s, 63 °C for 45 s, 72 °C for 1 min;
354 final extension at 72 °C for 10 min; hold at 4 °C.
355
356 ***Reagents***
357 Cannabinoid-based treatments included Δ⁹-tetrahydrocannabinol (THC, THC Pharm),
358 cannabidiol (CBD), methanandamide (mAEA, Cayman Chemical, #90050), a high-THC cannabis
359 extract, and a balanced THC:CBD (1:1) extract (kind gift from Dr. Paola Pineda, Grupo Curativa,
360 Colombia). Selective cannabinoid receptor inverse agonists included SR141716A (CB1R, SR1,
361 Tocris Bioscience, #0923) and SR144528 (CB2R, SR2, Tocris Bioscience, #1464). Tamoxifen
362 (Sigma, T5648) was used as a reference endocrine therapy. Stock solutions were prepared for a
363 final 1:1000 dilution. mAEA was dissolved in ethanol; all other compounds (THC, CBD, extracts,

364 SR1, SR2, and tamoxifen) were dissolved in DMSO. Vehicle controls were included in all
365 experiments using matched volumes of the respective solvents (DMSO or ethanol) in the culture
366 medium.
367
368 ***Primary tumor cell isolation and culture***
369 PyMT mice were euthanized at 6–8 weeks of age upon development of palpable tumors.
370 Tumors were excised and placed on ice in tumor cell medium consisting of DMEM (Corning, 10-
371 017-CV) supplemented with 1× GlutaMAX (Invitrogen, 12634-034), 10% FBS (Gibco, A5256701),
372 and antibiotics. Under aseptic conditions, tumors were minced into small fragments using a sterile
373 scalpel. Minced tissue was incubated in 5 mL of freshly prepared digestion solution (tumor
374 medium supplemented with 0.125 mg/mL Collagenase [Sigma, C9407] and 0.125 mg/mL Dispase
375 II [Gibco, 17105041]), prewarmed to 37 °C. The suspension was digested at 37 °C with agitation
376 (150 rpm) for 2 hours. Post-digestion, the mixture was filtered through a 100 μm cell strainer to
377 remove debris, centrifuged at 400 x g, and resuspended in fresh tumor medium. Cells were plated
378 and incubated at 37 °C for 20 minutes to promote adherence. Non-adherent cells were removed
379 by washing to eliminate fibroblasts and stromal contaminants. Fresh medium was then added.
380 Primary tumor cells were confirmed as epithelial by positive staining for pan-cytokeratin (Abcam,
381 ab7753). Cultures were maintained at 37 °C in a humidified incubator with 5% CO_2, tested weekly
382 for mycoplasma contamination, and passaged every 4 days upon reaching confluence.
383
384 ***Generation and culture of mammary tumor organoids***
385 PyMT, PyMT:CB2R^{-}/$^{-}$, and MMTV-neu mice were euthanized at 6–8 weeks of age, and
386 tumors were harvested for organoid generation. Organoids were established and maintained as
387 previously described (5). Briefly, excised tumors were minced and digested in pre-warmed
388 digestion solution consisting of DMEM supplemented with 1× GlutaMAX, 1% FBS, antibiotics
389 (referred to as wash medium), 0.125 mg/mL collagenase, and 0.125 mg/mL Dispase II. The tissue
390 suspension was incubated at 37 °C with constant shaking (150 rpm) for 2 hours. Following
391 enzymatic digestion, the cell suspension underwent sequential centrifugation at 500 × g to wash
392 away adipose tissue remnants using cold wash medium. The resulting pellet was resuspended in
393 basal medium composed of Advanced DMEM/F-12 (Invitrogen, 12634-034), 1× GlutaMAX, 10

394 mM HEPES (Invitrogen, 15630-056), and antibiotics, then centrifuged again at 500 × g. Pellets
395 were carefully resuspended in 10 mg/mL cold Cultrex growth factor-reduced Basement
396 Membrane Extract (BME) Type 2 (Trevigen, 3533-010-02), and 40 µL domes were plated in pre-
397 warmed 24-well plates. After the BME solidified, 650–1000 µL of pre-warmed breast cancer (BC)
398 organoid expansion medium was added to each well. The expansion medium was prepared by
399 supplementing the basal medium with the following components: 10% homemade R-Spondin-1
400 conditioned medium, 1× B27 supplement (Gibco, 17504-044), 1× N2 supplement (Gibco, 17-502-
401 001), 10 mM nicotinamide (Sigma, N0636), 1.25 mM N-acetylcysteine (Sigma, A9165), 10 nM
402 Gastrin I (Sigma, G9145), 100 ng/mL FGF10 (Peprotech, 100-26), 50 ng/mL Noggin (Peprotech,
403 120-10C), 50 ng/mL EGF (Peprotech, AF-100-15), 5 nM Neuregulin-1 (Peprotech, 100-03), 5 µM
404 Y-27632 (Abmole), 500 nM A83-01 (Tocris, 2939), 500 nM SB202190 (Sigma, S7067), and
405 Primocin (Invitrogen, Ant-pm-1). Organoids were passaged weekly, and expansion medium was
406 refreshed every two days. For cannabinoid treatment, organoids were exposed for four days to
407 compounds dissolved in DMSO at the following concentrations: 1 nM to 5 µM Δ9-THC, 10 nM
408 CBD, 10 nM THC-rich plant extract, 5 nM:5 nM THC:CBD 1:1 plant extract, 100 nM SR1, 100 nM
409 SR2, and 10 nM methanandamide (mAEA). Unless otherwise specified in the figure legends or
410 text, all analyses were conducted 10 days after treatment withdrawal.
411
412 ***Generation and culture of breast cancer patient-derived organoids***
413 Patient-derived tumor samples were minced and digested as previously described (5),
414 using a pre-warmed digestion solution at 37 °C with constant shaking (150 rpm) for 2 hours. The
415 resulting suspension underwent sequential centrifugation at 500 × g. Cells were then carefully
416 resuspended in BME, and 20 µL drops were plated in pre-warmed 24-well plates. After the
417 Matrigel solidified, patient breast cancer (BC) organoid expansion medium was added. The
418 patient BC organoid expansion medium consisted of basal medium supplemented with 20%
419 homemade R-Spondin-1 conditioned medium, 1× B27 supplement, 1× N2 supplement, 10 mM
420 nicotinamide, 1.25 mM N-acetylcysteine, 10 nM Gastrin I, 100 ng/mL FGF10, 100 ng/mL Noggin,
421 50 ng/mL EGF, 5 nM Neuregulin 1, 5 µM Y-27632, 500 nM A83-01, 500 nM SB202190, and
422 Primocin. Organoids were passaged every 7-10 days, and the BC organoid expansion medium

423 was refreshed every two days. Cannabinoid treatments, dissolved in DMSO, were applied to
424 organoids for four days.
425
426 ***Cancer-Associated Fibroblast (CAF) extraction and culture***
427 Mammary gland tumors were harvested from PyMT mice at 6–8 weeks of age for CAF
428 isolation, as previously described (55, 56). Tumors were minced into small fragments and
429 digested in a prewarmed solution containing wash medium supplemented with 0.125 mg/mL
430 collagenase, 0.125 mg/mL dispase II, and 0.1 mg/mL DNase I. The suspension was incubated at
431 37 °C with constant shaking (120 rpm) for 2 hours. Following digestion, the cell suspension was
432 filtered through a 100 µm strainer and centrifuged at 500 x g. The pellet was resuspended in
433 selection medium (DMEM with 10% FBS, 1× Insulin-Transferrin-Selenium [ITS-G; Gibco,
434 41400045], and antibiotics) and incubated for 30 minutes to allow selective fibroblast adherence.
435 After incubation, the medium was replaced with CAF culture medium (DMEM supplemented with
436 10% FBS, 1× GlutaMAX, and antibiotics). CAF identity was confirmed by immunostaining: cells
437 were vimentin-positive (BD Biosciences, 5505013) and cytokeratin-negative (Abcam, ab7753).
438
439 ***Peripheral Blood Mononuclear Cell (PBMC) isolation***
440 Peripheral blood was collected via cardiac puncture from adult PyMT tumor-bearing mice
441 and transferred to EDTA-coated tubes to prevent coagulation. Samples were diluted 1:2 in HBSS
442 (Gibco, 14025092). PBMCs were isolated by density gradient centrifugation using Ficoll-Paque™
443 PLUS (VWR, 17-1440-02), at a ratio of 1 mL Ficoll per 3 mL of diluted blood. The blood was
444 carefully layered over Ficoll and centrifuged at 1600 rpm for 27 minutes at room temperature (no
445 brake, low acceleration). The PBMC layer was collected, transferred to a clean tube, and washed
446 three times with PBS supplemented with 1% FBS and antibiotics. Cells were counted and
447 cryopreserved for subsequent co-culture experiments.
448
449 ***Mammary tumor organoid–CAF co-culture***
450 PyMT-derived organoids were dissociated and co-seeded with primary CAFs at a 1:250
451 organoid-to-CAF ratio. CAFs were harvested from confluent cultures by incubation with 0.25%
452 trypsin and 0.1% EDTA (Corning, 25-053-CI) for 4 minutes at 37 °C. Detached cells were

453 collected in CAF medium, centrifuged at 600 x g, and kept on ice until use. Simultaneously,
454 organoids were harvested by mechanical disruption and washed twice by centrifugation at 500 x
455 g. For co-culture, 250 CAFs per organoid were added to the organoid suspension, followed by
456 centrifugation at 500 x g. The resulting pellet was gently resuspended in cold BME, and 20 µL
457 drops were plated into prewarmed 8-well chamber slides (Ibidi, 80841). After BME polymerization
458 at 37 °C, 200–300 µL of prewarmed breast cancer organoid expansion medium was added per
459 well. As experimental controls, organoids were cultured under identical conditions either alone
460 (without fibroblasts) or co-seeded with NIH/3T3 fibroblasts (ATCC CRL-1658™) using the same
461 protocol and ratio. Co-cultures and controls were evaluated at days 4 and 10 and subsequently
462 analyzed by immunofluorescence staining.
463
464 ***Co-culture of organoids with CAFs and PBMCs under shear stress in a flow-controlled***
465 ***bioreactor***
466 PyMT-derived breast cancer organoids were dissociated and co-seeded with primary
467 CAFs and autologous PBMCs (isolated from the same mouse). Organoids and CAFs were
468 seeded at a 1:250 ratio into µ-Slide III 3D Perfusion chambers (Ibidi, 80371). Following seeding,
469 chambers were incubated with breast cancer organoid expansion medium for 2 hours at 37 °C in
470 a humidified atmosphere with 5% CO_2 to promote cell attachment. Chambers were then
471 connected to a flow-controlled bioreactor system (57). The system included a peristaltic pump
472 (ISMATEC MCP, 78002-00) equipped with an 8-roller, 12-channel pump head (ISMATEC Type
473 IBM733A, 78002-36) and 1.52 mm PharMed BPT tubing (95723-36). µ-Slides were linked using
474 Ibidi elbow luer connectors (10802) and serial connectors (10830) to sterile silastic tubing (Dow
475 Corning 515-012). Organoid–CAF co-cultures were exposed to continuous capillary-level
476 physiological shear stress (2.6 dyn/cm²). PBMCs were introduced into the circulating medium,
477 allowing dynamic interaction with the organoid–CAF co-culture. The following experimental
478 conditions were established: (1) Organoids alone under static conditions; (2) Organoids under
479 flow (shear stress only); (3) Organoid–CAF co-culture under flow; (4) Organoid–CAF–PBMC co-
480 culture under flow; (5) Organoid–CAF–PBMC co-culture under flow, treated with either THC or
481 SR2. Cultures were analyzed at days 4 and 10 post-seeding.
482

483 ***Mammary gland orthotopic injection in vivo***

484 PyMT-derived organoids were treated with 10 nM THC for 4 days. After 10 days of
485 cannabinoid withdrawal in culture, organoids were resuspended in basal medium and centrifuged
486 at 500 × g. The resulting pellets were dissociated into single cells by incubating them for 20
487 minutes with TrypLE Select enzyme (Gibco, 12563011) at 37 °C with agitation. A total of 1×10^4
488 organoid-derived cells in 100 µL (50 µL cell suspension and 50 µL BME) were orthotopically
489 injected into the left inguinal mammary fat pad of 6-week-old PyMT wild-type sister mice, which
490 served as controls for the organoid-derived injections. Tumor formation was first observed at
491 week 3 post-inoculation for control (organoid-derived) tumors, and at week 5 for THC-pretreated
492 organoid-derived tumors. Mice were monitored three times a week for tumor growth, with tumor
493 length measured using external calipers. Tumor volume was calculated using the formula: $(4\pi/3)$
494 $\times$ $(\text{width}/2)^2 \times (\text{length}/2)^2$. When tumors reached a volume of 1000 mm^3, mice were euthanized,
495 and tumors were excised for evaluation. Tumors were fixed in 10% formalin and prepared for
496 immunohistochemistry analysis.

497

498 ***Analysis of metastasis in vivo***

499 PyMT-derived organoids were differentiated using 10 nM THC for 4 days and
500 subsequently cultured for an additional 14 days. Organoids were then minced and dissociated
501 into a single-cell suspension by incubating with TrypLE for 20 minutes. A total of 5×10^5 organoid-
502 derived cells per mouse were injected into the lateral tail vein of 6-week-old PyMT wild-type mice
503 to induce lung metastasis. Mice were euthanized four weeks post-injection. Lungs were then
504 excised, fixed, and prepared for both immunohistochemistry and immunofluorescence analyses.

505

506 ***Secondary organoid formation assay***

507 Organoids were collected and dissociated into single cells to assess their self-renewal
508 and organoid-forming potential. Samples were centrifuged at 500 × g, and the resulting pellets
509 were incubated with pre-warmed TrypLE for 20 minutes at 37°C. Gentle mechanical dissociation
510 was performed every 5 minutes. After dissociation, the samples were centrifuged again at 500 ×
511 g. Single cells were resuspended in BME at a density of 1×10^4 cells per 40 µL and seeded into
512 a 24-well plate. Following cell seeding, 650–1000 µL of BC organoid expansion medium was

513 added to each well. Cells were maintained at 37°C in a humidified incubator with 5% CO_2. The
514 medium was refreshed every two days, and organoid formation was evaluated after 10 days in
515 culture.
516
517 ***Cell cycle analysis***
518 After completing the differentiation protocol, organoid cultures were harvested and
519 centrifuged at 500 x g. Organoids were dissociated into single cells by incubating with TrypLE
520 Select at 37ºC for 20 minutes, with gentle pipetting every 5 minutes. The dissociated cells were
521 then fixed in ice-cold 70% ethanol for 30 minutes on ice. After fixation, the cells were centrifuged
522 at 800 x g. To degrade RNA and enable selective DNA staining, fixed cells were incubated with
523 100 µg/ml RNAse A (Sigma, R5503). Following RNA degradation, 400 µl of 50 µg/ml propidium
524 iodide (Sigma, P-4170) was added per $1x10^6$ cells. The samples were incubated on ice for 10
525 minutes and then analyzed using a FACScalibur flow cytometer (BD Biosciences).
526
527 ***Fluorescence-Activated Cell Sorting and subsequent organoid culture of PyMT:CB2R***
528 ***tumors***
529 Mammary gland tumors from PyMT:CB2R$^{+/+}$, and PyMT:CB2R$^{-/-}$ mice were excised and
530 processed for flow cytometry analysis. Tumors were minced and enzymatically digested in
531 digestion solution (wash medium supplemented with 0.125 mg/mL Collagenase and 0.125 mg/mL
532 Dispase II) for one hour at 37°C with shaking at 180 rpm. For single-cell suspension, the digested
533 tissue was centrifuged at 600 × g and filtered through a 100 µm cell strainer using 10 mL of
534 blocking buffer (wash buffer supplemented with 5 mM EDTA). The suspension was centrifuged
535 again at 600 × g, and erythrocytes were lysed by incubating the sample for 15 minutes at room
536 temperature. After a second filtration through a 100 µm cell strainer, the sample was centrifuged
537 again at 600 × g and resuspended in FACS buffer (PBS supplemented with 2% FBS, 0.01%
538 sodium azide, and antibiotics) at a concentration of 1×10^6 cells per 100 µL. Fc receptors were
539 blocked by incubating the cells with anti-CD16/32 antibody (1:100) for 20 minutes on ice. After
540 blocking, cells were washed and resuspended at the same concentration for staining with the
541 following antibodies: EpCAM-FITC (BioLegend, 118207) at a 1:200 dilution and CD49f-Alexa
542 Fluor™ 647 (BioLegend, 313610) at a 1:20 dilution. Cells were incubated with the antibody mix

543 for 20 minutes on ice in the dark. After staining, samples were centrifuged at 1000 × g at 4°C and
544 resuspended in FACS buffer at a concentration of 1×10^6 cells in 100 µL, and stained with 7-AAD
545 (BioLegend, 420404) as a viability marker at a 1:50 dilution. Cells were sorted using a FACSAria
546 III cell sorter (BD Biosciences) into four distinct populations based on differential expression of
547 CD49f and EpCAM. FlowJo™ software was used for data analysis. Each population was collected
548 separately and used to initiate organoid cultures. Sorted cells were seeded at a density of 1×10^4
549 cells per well in 40 µL of BME in a pre-warmed 24-well plate. After matrix polymerization, 650–
550 1000 µL of BC organoid expansion medium was added to each well. Cultures were maintained
551 at 37°C with 5% CO_2, with unsorted cells serving as the control for organoid formation. Medium
552 was refreshed every 48 hours. Organoid formation was evaluated after 10 days in culture to
553 assess the growth potential of each sorted population.
554
555 ***Apoptosis assay by flow cytometry***
556 Organoid cultures were harvested and transferred to a tube for dissociation into single
557 cells. Pre-warmed TrypLE Select was used for cell dissociation, with incubation for 20 minutes at
558 37ºC. After digestion, cells were centrifuged at 500 x g. Apoptosis analysis was performed using
559 the Dead Cell Apoptosis Kit with Annexin V for Flow Cytometry (Invitrogen, V13445), according
560 to the manufacturer's instructions. Briefly, cells were stained with a 1:100 dilution of Annexin V-
561 Alexa Fluor™ 488 and 0.2 µg/ml propidium iodide (PI) solution in annexin-binding buffer. The
562 samples were incubated at room temperature for 15 minutes in the dark. Following incubation,
563 samples were analyzed using a FACScalibur flow cytometer.
564
565 ***Cell viability assay***
566 Organoids and primary tumor cells derived from PyMT mice were assessed for viability
567 based on intracellular ATP content using the CellTiter-Glo® 3D Cell Viability Assay (Promega,
568 G9682), following the manufacturer's instructions. Briefly, cells were lysed with the CellTiter-Glo
569 3D reagent, and luminescence was measured using an IVIS Spectrum system (PerkinElmer).
570 Background signals from the medium were subtracted, and relative luminescence units (RLU)
571 were normalized to control conditions.
572

573 ***Cellular migration analysis from patient-derived samples***

574 To investigate cellular migration traits in detail, we employed the HoloMonitor® M4, an
575 automated live-cell imaging cytometer that performs time-lapse analysis. This system allows for
576 the imaging and quantification of unstained, living cells directly within their culture vessels inside
577 the incubator, enabling real-time monitoring of various morphological and migratory parameters.
578 Based on digital holographic microscopy, the HoloMonitor measures phase shifts in light as it
579 passes through cells, which the software then uses to reconstruct high-resolution topographic
580 images. For our experiments, we used ibidi® plastic 24-well plates fitted with HoloLid™ lids—
581 specifically designed to reduce image artifacts caused by surface vibrations and condensation.
582 We quantified the following parameters: Cell area (μm²), the surface area occupied by each cell;
583 Irregularity, the degree to which a cell's outline deviates from a perfect circle; Migration (μm), the
584 shortest linear distance between a cell's initial and final positions; Motility (μm), the total path
585 length traveled by a cell; Motility speed (μm/h), the motility distance divided by the observation
586 time. Statistical analyses were performed using R software (version 4.5.0, RCore2013). For each
587 parameter, we calculated the mean ± standard error of the mean (SEM). A generalized linear
588 model (glm) (58) was fitted to assess the impact of experimental conditions, time and their
589 interaction on each variable. Variables were log transformed to verify assumptions of normality
590 and homoscedasticity.

591

592 ***Cytokine profiling from co-culture conditioned media***

593 Cytokine secretion profiles from co-culture conditions were analyzed using the Proteome
594 Profiler Mouse Cytokine Array Kit, Panel A (R&D Systems, ARY006), according to the
595 manufacturer's protocol. Briefly, 1 mL of conditioned media was collected from cell cultures,
596 centrifuged at 500 x g to remove cellular debris, and the supernatants were transferred to fresh
597 tubes and stored at -20°C until processing. Array membranes were blocked and incubated with
598 the Detection Antibody Cocktail. The antibody-sample mixture was applied to the membranes,
599 which were incubated overnight at 4°C. The following day, membranes were washed, incubated
600 with Streptavidin-HRP for 30 minutes, and developed using a chemiluminescent reagent. Signals
601 were detected using the ChemiDoc XRS+ Imaging System (BioRad). Cytokine spot intensities
602 were quantified using Fiji (ImageJ) and normalized to positive controls.

603 ***Immunofluorescence***

604 For immunofluorescence analysis, organoids were seeded into 8-well chamber slides
605 with removable wells (Nunc™ Lab-Tek™ II Chamber Slide™ System 154534) during the final
606 week of the culture period. Cells were briefly rinsed with phosphate-buffered saline (PBS) prior to
607 fixation. Organoids were fixed with 10% formalin for 1 hour at room temperature (RT).
608 Permeabilization was performed using 3% Triton X-100 (Sigma, T9284) in PBS for 20 minutes,
609 followed by three washes with 0.1% Triton X-100 in PBS. Blocking was carried out with blocking
610 solution (PBS + 0.1% Triton X-100 + 2% bovine serum albumin (BSA) [Sigma, A6003]) for 2.5
611 hours at RT. Primary antibodies were diluted in the blocking solution and added to the samples,
612 which were then incubated overnight at 4°C. After incubation, samples were washed with PBS,
613 and secondary antibodies were applied at a 1:500 dilution in the blocking solution. Incubation with
614 secondary antibodies was done at RT for 1.5 hours in dark conditions. After secondary antibody
615 incubation, samples were washed twice with PBS. For nuclear staining, DAPI was diluted 1:1000
616 in PBS and added to each well for a 10-minute incubation. After staining, the cells were mounted
617 using Mowiol 4-88 (Calbiochem, 475904) as the mounting medium. The primary antibodies used
618 for IF staining and their respective dilutions are as follows: **Cytokeratin 14** (rabbit monoclonal
619 EPR17350, Abcam, ab181595) at 1:100 dilution. **Cytokeratin 8/18** (mouse monoclonal TROMA-
620 I, DSHB, ab_531826) at 1:100 dilution. **Ki67** (mouse monoclonal B56, BD Biosciences, 550609)
621 at 1:400 dilution. **E-cadherin** (rabbit monoclonal 24E10, Cell Signaling, 3195S) at 1:500 dilution.
622 **Snail** (mouse monoclonal L70G2, Cell Signaling, 3895) at 1:250 dilution. **CD49f-Alexa Fluor™**
623 **647** (rat monoclonal GoH3, BioLegend, 313610) at 1:100 dilution. **EpCAM** (rat monoclonal G8.8,
624 BioLegend, 118207) at 1:200 dilution. **SOX10** (rabbit monoclonal EPR4007, Abcam, ab155279)
625 at 1:250 dilution. **CD24-Alexa Fluor™ 488** (rat monoclonal M1/69, BioLegend, 101816) at 1:800
626 dilution. **H3K9me3** (rabbit polyclonal, Abcam, ab8898) at 1:400 dilution. **H3K4me3** (rabbit
627 monoclonal EPR20551-225, Abcam, ab213224) at 1:100 dilution. **H3K27me3** (mouse
628 monoclonal, Abcam ab6002) at 1:200 dilution. **Phalloidin-Rhodamine** (Invitrogen R415) at 1:200
629 dilution. Samples were examined using a TCS SP8 laser scanning confocal microscope (Leica).
630 Image acquisition was performed in a sequential scanning mode by optimizing lasers and spectral
631 detectors for each specific fluorescent dye. Z-stacks were obtained by 2.5 µm z-steps, a 20X oil
632 immersion objective and a 1024x1024 scanning resolution. Image processing and analyses were

633 performed using Fiji (ImageJ). 3D projections were generated using the brightest point projection
634 method.
635
636 ***Immunohistochemistry***
637 Mammary gland and lung tissue samples were fixed in 10% formalin, paraffin-embedded,
638 and sectioned at 4 µm. The sections were mounted on Superfrost Plus slides and dried overnight.
639 Slides were stained with hematoxylin and eosin (H&E) or subjected to immunohistochemical
640 analysis. Antigen retrieval was performed, followed by blocking of endogenous peroxidase activity
641 using 3% hydrogen peroxide. The slides were then incubated with primary antibodies specific for
642 the following targets: **Cytokeratin 14** (rabbit polyclonal AF64, Covance, PRB-155P), **Cytokeratin**
643 **8/18** (rabbit monoclonal, Dako, IR094), **SOX9** (rabbit polyclonal, Millipore, AB5535), **SOX10** (goat
644 polyclonal N-20, Santa Cruz, c-17342), **Ki-67** (rabbit monoclonal D3B5, Cell Signaling, 12202),
645 and **Estrogen Receptor alpha** (mouse monoclonal CRET94D/H9). Secondary antibodies,
646 conjugated with horseradish peroxidase (OmniRabbit, Ventana, Roche), were applied, and the
647 immunohistochemical reaction was developed using 3,3'-diaminobenzidine tetrahydrochloride
648 (DAB) as the chromogen (Chromomap DAB, Ventana, Roche or DAB solution, Dako). Nuclei
649 were counterstained with Carazzi's hematoxylin. Finally, the slides were dehydrated, cleared, and
650 mounted with a permanent mounting medium for microscopic evaluation.
651
652 ***RNA extraction and analysis of mRNA levels***
653 RNA was extracted using NucleoZOL™ (Takara Bio) following the manufacturer's
654 instructions. Reverse transcription (RT) was performed from 1 µg of RNA using the Transcriptor
655 First Strand cDNA Synthesis Kit (Roche, 04379012001) with random hexamer primers.
656 Quantitative real-time PCR was then conducted using the PowerUp™ SYBR™ Green Master Mix
657 (Applied Biosystems, A25742), following the manufacturer's guidelines, using 50 ng of cDNA per
658 well in a 384-well plate. Data were acquired with a QuantStudio™ 12K Flex system (Applied
659 Biosystems). The following primers were used (5′−3′ sequence; F: Forward, R: Reverse): **Krt5**.
660 F: TCC TGT TGA ACG CCG CTG AC; R: CGG AAG GAC ACA CTG GAC TGG; **Krt14**. F: CAG
661 CCC CTA CTT CAA GAC CA; R: GTC GAT CTG CAG GAG GAC AT; **Krt8**. F: GGA CAT CGA
662 GAT CAC CAC CT; R: TGA AGC CAG GGC TAG TGA GT; **Krt18**. F: CAA GTC TGC CGA AAT

663 CAG GGA C; R: TCC AAG TTG ATG TTC TGG TTT T; **Cdh1**. F: AGG AAA TGC ACC CCT CCA
664 AT; R: AAT CGG CCA GCA TTT TCT G; **Cdh2**. F: GCC ATC ATC GCT ATC CTT CT; R: CCG
665 TTT CAT CCA TAC CAC AAA; **Vimentin**. F: CCA ACC TTT TCT TCC CTG AAC; R: TTG AGT
666 GGG TGT CAA CCA GA; **Sox10**. F: ATC AGC CAC GAG GTA ATG TCC AAC; R: ACT GCC
667 CAG CCC GTA GCC; **EpCAM**. F: GAT TCT GCA CGT GAG ACC TG; R: GAT ACC AAG TCA
668 AAC CGA GAA CTT.
669
670 ***RNA sequencing***
671 RNA was extracted using Nucleozol™ following the manufacturer's instructions. RNA-
672 seq sample preparation and initial data analysis were carried out by Novogene. In brief,
673 transcriptome libraries were generated from high-quality RNA samples (triplicates), which were
674 verified using the Agilent Bioanalyzer 2100. Messenger RNA was isolated using poly-T oligo-
675 attached magnetic beads, then fragmented prior to cDNA synthesis. Both non-stranded and
676 strand-specific libraries were prepared according to standard Illumina protocols. Library quality
677 was assessed using Qubit, qPCR, and Bioanalyzer analysis. Sequencing was performed on an
678 Illumina platform utilizing sequencing-by-synthesis technology to generate high-throughput reads.
679 Bioinformatic analysis began with quality control of raw reads using FastQC. Clean reads were
680 mapped to the reference genome with HISAT2. Differential expression was analyzed using
681 DESeq2, applying a threshold of adjusted $p \leq 0.05$ and $|\log2FC| \geq 1$. Functional enrichment was
682 performed using the clusterProfiler R package, with analysis across GO, KEGG, Reactome, DO,
683 and DisGeNET databases.
684
685 ***Statistical analysis***
686 All experiments were performed with at least three independent biological replicates.
687 Data are presented as mean ± SEM, and p-values ≤ 0.05 were considered statistically significant.
688 For comparisons between two independent groups, a two-tailed Student's t-test was used.
689 Correlations between two variables were calculated using Pearson's r. For multi-group
690 comparisons, data were analyzed using one-way ANOVA with post-hoc Tukey's multiple
691 comparison test, or two-way ANOVA when appropriate. Statistical analyses were performed using
692 GraphPad Prism software (version 10.1.2).

Data availability

RNAseq data has been deposited in the SRA repository under BioProject accession number PRJNA1276513.

Acknowledgements: We thank the CNIO Histopathology and Genomics Units, UCM Confocal Unit and UCM Animal Facility for their technical support. We are indebted to the members of the Cannabinoid Signaling group (UCM), Eva Resel for administrative support, and to our former undergraduate and master students, with special mention to Marc Pinto, Manuel Luque, and Paula Gijón. We would like to express our thanks to Novogene Europe for their technical and customer support, with special appreciation to Metehan Cifdaloz, Paula Yagüe, and Haozhen Su. We are also extremely grateful to the Hospital *La Paz*, particularly to the Gynecology and Histopathology Units, for their constructive participation in this work and very specially, to the patients enrolled in this research study. This work has been in part financed by benefactors, through multiple donations to *Asociación Española contra el Cáncer* (AECC). We are extremely thankful to all our anonymous donors. The work has been funded by the Spanish Ministry of Science, Innovation and Universities, supported with European Regional Development funds: **CNS2022-135364** and **PID2022-136508OA-I00**, and the Complutense University, through the project **PR3/23-30841** to MS-R. MS-R was also supported by AECC (**INVES18005SALA**) and a *Ramón y Cajal* contract from the Ministry of Science, Innovation and Universities (**RYC2020-028929-I**). NGM-I was supported by AECC (**PRDMA19003GARC**) and Fulbright fellowship (**PS00380044**). ERE and MB were supported by National Institutes of Health (NIH) Research Project Grant **R01 HL 161069**.

Author contributions: NGM-I conducted most of the cellular and *in vivo* experiments, with assistance from GP-G, MR-H, CQ-G, EM-Z, and MS-R. The Flow Cytometry and Confocal Imaging Unit at UCM (LMA-C and CH) collaborated on confocal imaging analyses and flow cytometry experiments. The Histopathology Unit at CNIO performed IHC experiments and provided professional histopathological analyses of the samples when needed (EC). MM-R and AZ-C contributed to RNA sequencing experiments, with support from NGM-I, CQ-G, and MS-R. AP-P collaborated with EM-Z and NGM-I to perform the R analysis of patient-derived data. LF-A

723 assisted in preparing the necessary documents and protocols for patient enrollment at the
724 hospital, recruited patients, and offered clinical advice. CS, MB-C and ERE provided guidance,
725 materials and/or resources. MB-C and ERE directly contributed to the optimization and execution
726 of dynamic cell co-culture experiments alongside NGM-I. MS-R and NGM-I supervised the project
727 design, data evaluation and analysis. MS-R conceived the study, managed the teamwork and
728 wrote the manuscript with contributions from the primary authors.
729
730 **Competing interest:** The authors declare no competing financial interests.
731
732 **Ethical approvals:** All animal procedures were conducted at the Animal Facility of the Faculty of
733 Biology, Complutense University of Madrid (UCM). The experimental protocols involving animals
734 adhered to local regulations (RD53/2013 and ECC/566/2015) and were approved by the relevant
735 Regulatory Agencies, including Complutense University and the Community of Madrid. All authors
736 involved in animal experimentation hold the necessary accreditation (categories C and D) granted
737 by the Competent Authority: CAP-T-0771-15, CAM Animal Welfare Committee on Animal
738 Experimentation. Regarding patient protection, all procedures followed the guidelines of Hospital
739 La Paz, local regulations, and the Declaration of Helsinki, as well as the Guidelines for Good
740 Clinical Practice (GCP) established by the International Conference on Harmonization (ICH E6).
741 The protocols for sample collection, processing, and any additional materials provided to the
742 patients (e.g., Patient Information Sheets and the Informed Consent Document) were approved
743 by the Clinical Research Ethics Committee of *Hospital La Paz*, in full compliance with national
744 legislation.

745 **References**

746 1. Hanahan D. Hallmarks of Cancer: New Dimensions. Cancer Discov. 2022;12(1):31-46.
747
748 2. de The H. Differentiation therapy revisited. Nat Rev Cancer. 2018;18(2):117-27.
749
750 3. Sole R, Aguade-Gorgorio G. The ecology of cancer differentiation therapy. J Theor Biol.
751 2021;511:110552.
752
753 4. Kim SI, Sohn J, Koo JS, Park SH, Park HS, Park BW. Molecular subtypes and tumor
754 response to neoadjuvant chemotherapy in patients with locally advanced breast cancer.
755 Oncology. 2010;79(5-6):324-30.
756
757 5. Martinez-Illescas NG, Leal S, Gonzalez P, Grana-Castro O, Munoz-Oliveira JJ, Cortes-
758 Pena A, et al. miR-203 drives breast cancer cell differentiation. Breast Cancer Res.
759 2023;25(1):91.
760
761 6. Salazar-Roa M, Trakala M, Alvarez-Fernandez M, Valdes-Mora F, Zhong C, Munoz J, et
762 al. Transient exposure to miR-203 enhances the differentiation capacity of established pluripotent
763 stem cells. EMBO J. 2020;39(16):e104324.
764
765 7. Dreesen O, Brivanlou AH. Signaling pathways in cancer and embryonic stem cells. Stem
766 Cell Rev. 2007;3(1):7-17.
767
768 8. Hanahan D, Weinberg RA. The hallmarks of cancer. Cell. 2000;100(1):57-70.
769
770 9. Batlle E, Clevers H. Cancer stem cells revisited. Nat Med. 2017;23(10):1124-34.
771 10. Takebe N, Harris PJ, Warren RQ, Ivy SP. Targeting cancer stem cells by inhibiting Wnt,
772 Notch, and Hedgehog pathways. Nat Rev Clin Oncol. 2011;8(2):97-106.
773
774 11. Takebe N, Ivy SP. Controversies in cancer stem cells: targeting embryonic signaling
775 pathways. Clin Cancer Res. 2010;16(12):3106-12.
776
777 12. Liu J, Xiao Q, Xiao J, Niu C, Li Y, Zhang X, et al. Wnt/beta-catenin signalling: function,
778 biological mechanisms, and therapeutic opportunities. Signal Transduct Target Ther. 2022;7(1):3.
779
780 13. Nwabo Kamdje AH, Takam Kamga P, Tagne Simo R, Vecchio L, Seke Etet PF, Muller
781 JM, et al. Developmental pathways associated with cancer metastasis: Notch, Wnt, and
782 Hedgehog. Cancer Biol Med. 2017;14(2):109-20.

783

14. Bolos V, Grego-Bessa J, de la Pompa JL. Notch signaling in development and cancer. Endocr Rev. 2007;28(3):339-63.

15. Huang JJ, Blobe GC. Dichotomous roles of TGF-beta in human cancer. Biochem Soc Trans. 2016;44(5):1441-54.

16. Larue L, Bellacosa A. Epithelial-mesenchymal transition in development and cancer: role of phosphatidylinositol 3' kinase/AKT pathways. Oncogene. 2005;24(50):7443-54.

17. Rah B, Rather RA, Bhat GR, Baba AB, Mushtaq I, Farooq M, et al. JAK/STAT Signaling: Molecular Targets, Therapeutic Opportunities, and Limitations of Targeted Inhibitions in Solid Malignancies. Front Pharmacol. 2022;13:821344.

18. Hinz B, Ramer R. Cannabinoids as anticancer drugs: current status of preclinical research. Br J Cancer. 2022;127(1):1-13.

19. Ligresti A, De Petrocellis L, Di Marzo V. From Phytocannabinoids to Cannabinoid Receptors and Endocannabinoids: Pleiotropic Physiological and Pathological Roles Through Complex Pharmacology. Physiol Rev. 2016;96(4):1593-659.

20. Maccarrone M. Missing Pieces to the Endocannabinoid Puzzle. Trends Mol Med. 2020;26(3):263-72.

21. Ramer R, Schwarz R, Hinz B. Modulation of the Endocannabinoid System as a Potential Anticancer Strategy. Front Pharmacol. 2019;10:430.

22. Velasco G, Sanchez C, Guzman M. Towards the use of cannabinoids as antitumour agents. Nat Rev Cancer. 2012;12(6):436-44.

23. Gaoni Y, Mechoulam R. Isolation, Structure, and Partial Synthesis of an Active Constituent of Hashish. J Am Chem Soc. 1964;86(8):1646-+.

24. Oesch S, Gertsch J. Cannabinoid receptor ligands as potential anticancer agents--high hopes for new therapies? J Pharm Pharmacol. 2009;61(7):839-53.

25. Guzman M, Duarte MJ, Blazquez C, Ravina J, Rosa MC, Galve-Roperh I, et al. A pilot clinical study of Delta9-tetrahydrocannabinol in patients with recurrent glioblastoma multiforme. Br J Cancer. 2006;95(2):197-203.

26. Dumitru CA, Sandalcioglu IE, Karsak M. Cannabinoids in Glioblastoma Therapy: New Applications for Old Drugs. Front Mol Neurosci. 2018;11:159.

27. Twelves C, Sabel M, Checketts D, Miller S, Tayo B, Jove M, et al. A phase 1b randomised, placebo-controlled trial of nabiximols cannabinoid oromucosal spray with temozolomide in patients with recurrent glioblastoma. Br J Cancer. 2021;124(8):1379-87.

28. Bhaskaran D, Savage J, Patel A, Collinson F, Mant R, Boele F, et al. A randomised phase II trial of temozolomide with or without cannabinoids in patients with recurrent glioblastoma (ARISTOCRAT): protocol for a multi-centre, double-blind, placebo-controlled trial. BMC Cancer. 2024;24(1):83.

29. Willyard C. Cancer therapy: an evolved approach. Nature. 2016;532(7598):166-8.

30. Perez-Gomez E, Andradas C, Blasco-Benito S, Caffarel MM, Garcia-Taboada E, Villa-Morales M, et al. Role of cannabinoid receptor CB2 in HER2 pro-oncogenic signaling in breast cancer. J Natl Cancer Inst. 2015;107(6):djv077.

31. Raina K, Dey C, Thool M, Sudhagar S, Thummer RP. An Insight into the Role of UTF1 in Development, Stem Cells, and Cancer. Stem Cell Rev Rep. 2021;17(4):1280-93.

32. Jia J, Zheng X, Hu G, Cui K, Zhang J, Zhang A, et al. Regulation of pluripotency and self-renewal of ESCs through epigenetic-threshold modulation and mRNA pruning. Cell. 2012;151(3):576-89.

33. Gatenby RA, Silva AS, Gillies RJ, Frieden BR. Adaptive therapy. Cancer Res. 2009;69(11):4894-903.

34. Early Breast Cancer Trialists' Collaborative G, Davies C, Godwin J, Gray R, Clarke M, Cutter D, et al. Relevance of breast cancer hormone receptors and other factors to the efficacy of adjuvant tamoxifen: patient-level meta-analysis of randomised trials. Lancet. 2011;378(9793):771-84.

35. Pierce GB, Wallace C. Differentiation of malignant to benign cells. Cancer Res. 1971;31(2):127-34.

36. Huang ME, Ye YC, Chen SR, Chai JR, Lu JX, Zhoa L, et al. Use of all-trans retinoic acid in the treatment of acute promyelocytic leukemia. Blood. 1988;72(2):567-72.

862 37. Cruz FD, Matushansky I. Solid tumor differentiation therapy - is it possible? Oncotarget.
863 2012;3(5):559-67.
864
865 38. Pagano C, Navarra G, Coppola L, Avilia G, Bifulco M, Laezza C. Cannabinoids:
866 Therapeutic Use in Clinical Practice. Int J Mol Sci. 2022;23(6).
867
868 39. Galve-Roperh I, Sanchez C, Cortes ML, Gomez del Pulgar T, Izquierdo M, Guzman M.
869 Anti-tumoral action of cannabinoids: involvement of sustained ceramide accumulation and
870 extracellular signal-regulated kinase activation. Nat Med. 2000;6(3):313-9.
871
872 40. Pyszniak M, Tabarkiewicz J, Luszczki JJ. Endocannabinoid system as a regulator of
873 tumor cell malignancy - biological pathways and clinical significance. Onco Targets Ther.
874 2016;9:4323-36.
875
876 41. Liu WM, Scott KA, Shamash J, Joel S, Powles TB. Enhancing the in vitro cytotoxic activity
877 of Delta9-tetrahydrocannabinol in leukemic cells through a combinatorial approach. Leuk
878 Lymphoma. 2008;49(9):1800-9.
879
880 42. Kampa-Schittenhelm KM, Haverkamp T, Bonin M, Tsintari V, Buhring HJ, Haeusser L, et
881 al. Epigenetic activation of O-linked beta-N-acetylglucosamine transferase overrides the
882 differentiation blockage in acute leukemia. EBioMedicine. 2020;54:102678.
883
884 43. Sido JM, Yang X, Nagarkatti PS, Nagarkatti M. Delta9-Tetrahydrocannabinol-mediated
885 epigenetic modifications elicit myeloid-derived suppressor cell activation via STAT3/S100A8. J
886 Leukoc Biol. 2015;97(4):677-88.
887
888 44. Tomko AM, Whynot EG, Ellis LD, Dupre DJ. Anti-Cancer Potential of Cannabinoids,
889 Terpenes, and Flavonoids Present in Cannabis. Cancers (Basel). 2020;12(7).
890 45. Mangal N, Erridge S, Habib N, Sadanandam A, Reebye V, Sodergren MH. Cannabinoids
891 in the landscape of cancer. J Cancer Res Clin Oncol. 2021;147(9):2507-34.
892
893 46. Howlett AC, Barth F, Bonner TI, Cabral G, Casellas P, Devane WA, et al. International
894 Union of Pharmacology. XXVII. Classification of cannabinoid receptors. Pharmacol Rev.
895 2002;54(2):161-202.
896
897 47. Begbie J, Doherty P, Graham A. Cannabinoid receptor, CB1, expression follows neuronal
898 differentiation in the early chick embryo. J Anat. 2004;205(3):213-8.
899

900 48. Mulder J, Aguado T, Keimpema E, Barabas K, Ballester Rosado CJ, Nguyen L, et al.
901 Endocannabinoid signaling controls pyramidal cell specification and long-range axon patterning.
902 Proc Natl Acad Sci U S A. 2008;105(25):8760-5.
903
904 49. Wang X, Dow-Edwards D, Keller E, Hurd YL. Preferential limbic expression of the
905 cannabinoid receptor mRNA in the human fetal brain. Neuroscience. 2003;118(3):681-94.
906
907 50. Pagano C, Navarra G, Coppola L, Bifulco M, Laezza C. Molecular Mechanism of
908 Cannabinoids in Cancer Progression. Int J Mol Sci. 2021;22(7).
909
910 51. Okuda A, Fukushima A, Nishimoto M, Orimo A, Yamagishi T, Nabeshima Y, et al. UTF1,
911 a novel transcriptional coactivator expressed in pluripotent embryonic stem cells and extra-
912 embryonic cells. EMBO J. 1998;17(7):2019-32.
913
914 52. Lou Y, Jin S, Hong X, Hong Z, Xu C. Expression and clinical significance of
915 undifferentiated embryonic cell transcription factor 1 in breast cancer. Transl Cancer Res.
916 2023;12(1):150-62.
917
918 53. Wu XL, Zheng PS. Undifferentiated embryonic cell transcription factor-1 (UTF1) inhibits
919 the growth of cervical cancer cells by transactivating p27Kip1. Carcinogenesis. 2013;34(7):1660-
920 8.
921
922 54. Smoum R, Grether U, Karsak M, Vernall AJ, Park F, Hillard CJ, et al. Editorial:
923 Therapeutic potential of the cannabinoid CB2 receptor. Front Pharmacol. 2022;13:1039564.
924
925 55. Primac I, Maquoi E, Blacher S, Heljasvaara R, Van Deun J, Smeland HY, et al. Stromal
926 integrin alpha11 regulates PDGFR-beta signaling and promotes breast cancer progression. J Clin
927 Invest. 2019;129(11):4609-28.
928
929 56. Sharon Y, Alon L, Glanz S, Servais C, Erez N. Isolation of normal and cancer-associated
930 fibroblasts from fresh tissues by Fluorescence Activated Cell Sorting (FACS). J Vis Exp.
931 2013(71):e4425.
932
933 57. Salazar-Martin AG, Kalluri AS, Villanueva MA, Hughes TK, Wadsworth MH, 2nd, Dao TT,
934 et al. Single-Cell RNA Sequencing Reveals That Adaptation of Human Aortic Endothelial Cells to
935 Antiproliferative Therapies Is Modulated by Flow-Induced Shear Stress. Arterioscler Thromb Vasc
936 Biol. 2023;43(12):2265-81.
937

58. Bolker BM, Brooks ME, Clark CJ, Geange SW, Poulsen JR, Stevens MH, et al. Generalized linear mixed models: a practical guide for ecology and evolution. Trends Ecol Evol. 2009;24(3):127-35.

942 **Figure legends**

943

944 **Figure 1. A brief nanomolar THC exposure induces a long-term basal-to-luminal**
945 **morphological and molecular switch in MMTV-PyMT mammary tumor organoids. A**,
946 Schematic of the experimental design. PyMT-derived tumor organoids were treated with vehicle
947 (DMSO) or 10 nM THC for 4 days, followed by extended culture. Analyses were performed at 1-,
948 2-, and 3-weeks post-treatment. **B**, Representative brightfield images of control and THC-treated
949 organoids at 2 weeks. *n*=6 independent experiments. Scale bar, 100 µm. **C**, Confocal images of
950 organoids stained for CD24 (green) and CD49f (red) -cell surface markers of mammary gland
951 precursor- at 1, 2, and 3 weeks, showing temporal changes in morphology and marker expression
952 after THC exposure. DAPI (blue) stains nuclei. Upper panels show 3D stacks; lower panels show
953 representative single slices. *n*=3 independent experiments. Scale bar, 100 µm. **D**, Quantification
954 of organoids classified as granular (basal), mid (intermediate), or cystic (luminal/rounded) over
955 time. *n*=3 independent experiments; *p<0.05, **p<0.01, ***p<0.001 vs. control (granular);
956 #p=0.014 vs. control (cystic) (Two-way ANOVA). **E**, Quantification of organoid size (µm) at
957 endpoint. *n*=3 independent experiments; 80–100 organoids per condition; ****p<0.0001 (unpaired
958 Student's t-test). **F**, Confocal images of organoids at 2 weeks stained for CK14 (green; basal
959 marker) and CK8/18 (red; luminal marker). Left: 3D stacks; middle: single slices; right: merged
960 with brightfield. DAPI (blue) stains nuclei. *n*=4 independent experiments. Scale bar, 100 µm. **G**,
961 qPCR analysis of cytokeratin genes (CK14/5 and CK8/18, denoting a basal-like and luminal-like
962 phenotypes, respectively) at endpoint, normalized to GAPDH. *n*=3 independent experiments;
963 *p<0.05, **p<0.01 (unpaired Student's t-test).

964

965 **Figure 2. Brief exposure to nanomolar THC prevents collective migration, promotes**
966 **mesenchymal-to-epithelial transition, and reduces self-renewal in mammary tumor**
967 **organoids. A,** Representative confocal images of basal organoids showing collective migration
968 in control cultures. Organoids are stained for E-CAD (green) and SNAIL (red) (left) -as EMT
969 markers- or CK14 (green) and CK8/18 (red) (right). Note the cellular projections extending from
970 the organoid edges and attaching to the substrate. The inset highlights preserved E-CAD staining
971 in migrating areas, indicating cohesive cell movement. DAPI (blue) stains nuclei. *n*=3 independent

experiments. Scale bar, 100 µm. **B**, Quantification of the two-dimensional area (µm²) of collective-migratory projections in control vs. THC-treated cultures at 2 weeks. *n*=3 independent experiments; 25–30 organoids per condition; ***p<0.001 (unpaired Student's t-test). Representative brightfield images (right) illustrate measured areas. Scale bar, 100 µm. **C**, qPCR analysis of EMT-related genes at day 14. mRNA levels were normalized to GAPDH. *n*=3 independent experiments; *p<0.05 (unpaired Student's t-test). **D**, Time-course comparison of organoids displaying collective migration in control vs. THC-treated conditions. *n*=3 independent experiments; *p<0.05 (unpaired Student's t-test). **E**, Quantification of secondary organoid formation from single-cell dissociation at 21 days, indicating self-renewal capacity. *n*=6 independent experiments; ***p<0.001 (unpaired Student's t-test). **F**, Confocal images of organoids stained for CD49f (red), EpCAM (green), and SOX10 (white; stemness marker) after treatment with vehicle or 10 nM THC and analyzed at 2 weeks. DAPI (blue) stains nuclei. Merged images with brightfield are shown on the right. *n*=4 independent experiments. Scale bar, 100 µm. **G**, qPCR analysis of stemness and differentiation markers (Sox10, EpCAM) at day 14. Data normalized to GAPDH. *n*=3 independent experiments; *p<0.05 (unpaired Student's t-test).

Figure 3. *In vivo* functional evidence of THC-induced tumor cell differentiation. **A**, Schematic of the experimental design. MMTV-PyMT-derived organoids were treated with vehicle or THC (10 nM) for 4 days, cultured drug-free for 10 days, and orthotopically injected into PyMT wild-type littermates. Mice (*n*=8 vehicle, *n*=8 THC) were monitored for 100 days to assess tumor onset and growth. **B**, Brightfield and immunofluorescence images of organoids treated as indicated and analyzed before injection. Organoids showed expected expression of basal (CK14; green) or luminal (CK8/18; red) markers. DAPI (blue) stains nuclei. Scale bar, 100 µm. **C**, Kaplan-Meier plot showing tumor onset (% of mice with tumors) over time. **p<0.01 (Two-way ANOVA). **D**, Quantification of tumor volume (mm³) in both groups. ****p<0.0001 (Two-way ANOVA). **E**, Histopathological classification of tumors at endpoint (100 days): expanded/focal infiltrating neoplasia, local neoplasia, hyperplasia, or no tumor cells. **p<0.01 (Two-way ANOVA). Right: H&E-stained images of representative infiltrating neoplasia (control) and localized hyperplasia (THC). Scale bar, 500 µm. **F**, Schematic of metastasis assay. Organoids were treated with vehicle or THC (10 nM) for 4 days, cultured for 2 additional weeks, and injected via tail vein into PyMT

1002 wild-type mice. Lung metastases were assessed one-month post-injection (*n*=9 vehicle, *n*=7
1003 THC). **G**, Distribution of micro- and macro-metastases in lung tissue per condition. *p<0.05 (Two-
1004 way ANOVA). Right: H&E-stained images of representative lung metastases. Scale bar, 500 µm.
1005 **H**, Quantification of micro-metastases per animal. Each dot represents one mouse. **p<0.01
1006 (Two-way ANOVA). **I**, Immunofluorescence of lung sections stained for CK14, indicating micro-
1007 metastases. DAPI (blue) stains nuclei. Scale bar, 500 µm.
1008
1009 **Figure 4. SR2, but not SR1, mimics THC in promoting a basal-to-luminal switch, blocking**
1010 **collective migration, and reducing self-renewal in mammary tumor organoids.**
1011 **A**, Representative brightfield images of organoids treated for 4 days with vehicle, THC (10 nM),
1012 SR1 (100 nM), or SR2 (100 nM), and analyzed after two weeks of drug withdrawal. *n*=4
1013 independent experiments. Scale bar, 100 µm. **B**, Quantification of organoid morphology (granular,
1014 mid, cystic) in each condition at 14 days. ***p<0.001; ****p<0.0001 (Two-way ANOVA, granular
1015 vs. control); #p<0.05; ####p<0.0001 (cystic vs. control). **C**, Organoid size (µm) measured at 14
1016 days. *n*=80–100 organoids/condition across 4 experiments; ****p<0.0001 (One-way ANOVA). **D**,
1017 Confocal images of organoids stained for CK14 (green) and CK8/18 (red), showing marker
1018 changes 2 weeks after treatment. DAPI (blue) stains nuclei; bottom panels show merged IF and
1019 brightfield images. *n*=4. Scale bar, 100 µm. **E**, Quantification of collective-migratory projection
1020 area (µm²) in all conditions at 2 weeks. *n*=25–30 organoids/condition; **p<0.01 (unpaired
1021 Student's *t*-test). **F**, Number of secondary organoids formed from single-cell dissociation
1022 (indicating self-renewal) at 21 days. *n*=3 independent experiments; *p<0.05; **p<0.01 (One-way
1023 ANOVA).
1024
1025 **Figure 5. THC and SR2 trigger early and reversible epigenetic remodeling, followed by later**
1026 **differentiation. A,** Schematic timeline of the experimental workflow. **B**, Volcano plots showing
1027 differentially expressed genes in organoids treated with THC (10 nM) or SR2 (100 nM) vs. vehicle
1028 at day 3 and day 14 post-treatment. Genes with $\log_2$ fold change between −1 and 1 are
1029 considered unchanged. *n*=3 independent experiments. **C,** Gene Ontology (GO) enrichment
1030 analysis at day 3 of treatment, showing epigenetic regulation pathways significantly altered in
1031 SR2-treated organoids compared to control. Normalized Enrichment Score (NES) and gene set

size are indicated. **D,** Gene Set Enrichment Analysis (GSEA) of pathways related to pluripotency (top) and Polycomb Repressive Complex 2 (PRC2; bottom) in SR2-treated vs. control organoids at day 3 of treatment. **E,** Dot plots showing KEGG pathway enrichment analysis of differentially expressed genes following THC (top) or SR2 (bottom) treatment and evaluated at day 14, providing rationale for therapeutic tamoxifen combination in ***Figure 7***. **F,** Violin plots showing expression scores of validated UTF1 (top) and PRC2 (bottom) targets at day 3 (32). **G,** Violin plots of the same gene sets as in (E) at day 14 post-treatment (32). **H-I,** Organoids stained for H3K9me3 (red) and phalloidin (cytoskeleton marker; yellow) in upper images; H3K4me3 (red), H3K27me3 (green) and phalloidin (yellow) in bottom images, at day 3 (**H**) and day 14 (**I**), with DAPI (blue) staining nuclei. Violin plots show quantification of total nuclear fluorescence intensity per nucleus (800-1500 nuclei were evaluated per condition) for every staining, and the H3K27me3/H3K4me3 ratio denotes chromatin bivalency. *n*=3 independent experiments. Scale bar, 100 µm.

Figure 6. THC and SR2 promote stable differentiation, remodeling organoid architecture, migration, and cytokine signaling in a 3D co-culture system under shear stress. A, Schematic of the experimental setup. Organoids embedded in BME were co-cultured with cancer-associated fibroblasts (CAFs) and exposed to circulating peripheral blood mononuclear cells (PBMCs), with continuous pumped flux inducing shear stress. Co-cultures were treated with vehicle, THC (10 nM), or SR2 (100 nM) for 4 days, followed by 10 days in drug-free media. Samples were analyzed at two time points as indicated. **B,** Quantification of organoid morphology (granular, mid, cystic) at day 10 across conditions. *n*=3 independent experiments; *p<0.05 vs. control (granular); $^{\#}$p<0.05 vs. control (cystic) (Two-way ANOVA). **C,** Organoid size (µm) measured at day 4 and day 10. *n*=3 independent experiments; **p<0.01; ***p<0.001; ****p<0.0001 (One-way ANOVA). **D,** Percentage of organoids exhibiting collective migration at day 4 and day 10 in each treatment condition. *n*=3 independent experiments; **p<0.01 (One-way ANOVA). **E,** Quantification of collective migratory projection area (µm²) across conditions at day 4 and day 10. *n*=3 independent experiments; **p<0.01 (One-way ANOVA). **F,** Streptavidin-HRP based analysis of cytokines and chemokines secreted into the culture medium at day 10 for each condition: PBMC alone (red) or organoids+PBMCs+CAFs treated with vehicle (yellow), THC

1062 (green) or SR2 (blue). *n*=3 independent experiments; **p<0.01 (One-way ANOVA). **G-H,** Confocal
1063 images of organoids at day 10 stained for H3K4me3 (red) and phalloidin (yellow) (**G**) and for
1064 H3K27me3 (green) and phalloidin (yellow) (**H**), with DAPI (blue) marking nuclei. Violin plots show
1065 the quantification of total nuclear fluorescence intensity per nucleus (800-1500 nuclei were
1066 evaluated per condition) for every staining, as indicated. *n*=3 independent experiments. Scale
1067 bar, 100 µm.
1068
1069 **Figure 7. Cannabinoid-induced differentiation enhances tamoxifen response by promoting**
1070 **basal-to-luminal switching and reducing tumor organoid fitness. A,** Schematic of the
1071 experimental design. MMTV-PyMT–derived organoids were pre-treated with vehicle, THC (10
1072 nM), or SR2 (100 nM) for 4 days, followed by 10 days in drug-free media. Tamoxifen (0.5 µM)
1073 was then administered for 4 days, and cultures were analyzed immediately or up to 2 weeks later.
1074 **B,** Flow cytometry analysis of apoptosis using PI and Annexin V, assessed immediately after
1075 tamoxifen exposure or 2 weeks later in pre-differentiated cultures. *n*=4 independent experiments;
1076 *p<0.05; **p<0.01; (Unpaired Student's t-test). **C,** Cell cycle profiles comparing tamoxifen alone
1077 to SR2 + tamoxifen at increasing doses (0–5 µM). Left: representative flow cytometry plots. Right:
1078 quantification of cell cycle phases (G1, S, G2/M). *n*=3 independent experiments. **D,** Quantification
1079 of organoid morphology at endpoint: granular (basal), mid-transition, or cystic (luminal). *n*=4
1080 independent experiments; **p<0.01; ***p<0.001 ****p<0.0001 (Two-way ANOVA). **E,** Organoid
1081 size (µm) at endpoint across treatment conditions. *n*=4; 80–100 organoids per condition; *p<0.05;
1082 **p<0.01; ****p<0.0001 (One-way ANOVA). **F,** Percentage of organoids exhibiting collective-
1083 migratory projections at endpoint. *n*=4; *p*-values as indicated (One-way ANOVA). **G,** Self-renewal
1084 capacity assessed by quantification of secondary organoids formed after single-cell dissociation.
1085 *n*=4 independent experiments; **p<0.01; ***p<0.001; ****p<0.0001 (One-way ANOVA).
1086
1087 **Figure 8. CB2R–tamoxifen combination enhances therapy efficacy in patient-derived**
1088 **breast cancer organoids**. **A**, Experimental workflow. Surgical specimens were used to establish
1089 patient-derived organoid cultures. After expansion, organoids were treated with vehicle or SR2
1090 (100 nM) for 4 days, followed by a 10-day drug-free period. Prior to tamoxifen treatment, cell
1091 dispersal from organoids was assessed using dynamic holographic imaging. Tamoxifen (5 µM)

1092 was then administered for 4 days. Organoids were analyzed two weeks later to evaluate
1093 cooperative effects on self-renewal. *n*=2 independent tumors, 3 technical replicates each. **B**,
1094 Representative holographic images showing 2D movement of organoid-derived cells treated with
1095 vehicle or SR2 (100 nM), assessed in a wound healing assay at different time points. **C–F**,
1096 Quantification of wound healing assay parameters: cell area (μm²) (**C**), irregularity (**D**), migration
1097 distance (μm) (**E**), and motility (μm) (**F**) under both treatment conditions. A linear model was fitted
1098 to assess the impact of experimental conditions on each variable. Statistics shown in **Supp.**
1099 **Figure 8**. **G**, Confocal images of organoids stained for E-cadherin (green) and Snail (red),
1100 analyzed 10 days post-differentiation. Nuclei were stained with DAPI (blue). Shown are
1101 representative 3D confocal stacks. Scale bar = 100 μm. **H**, Quantification of organoid size (μm)
1102 at day 10 post-differentiation. ****$p < 0.0001$ (one-way ANOVA). **I**, Percentage of organoids
1103 displaying collective migration at day 10 post-differentiation. **J**, Total number of secondary
1104 organoids formed after single-cell disaggregation, reflecting self-renewal capacity, measured two
1105 weeks after tamoxifen treatment. ***$p < 0.001$ (one-way ANOVA). **K**, Representative brightfield
1106 images of organoids at different time points: 10 days after differentiation, and 5 or 20 days after
1107 tamoxifen treatment, following the experimental timeline shown in (A).

Figure 1

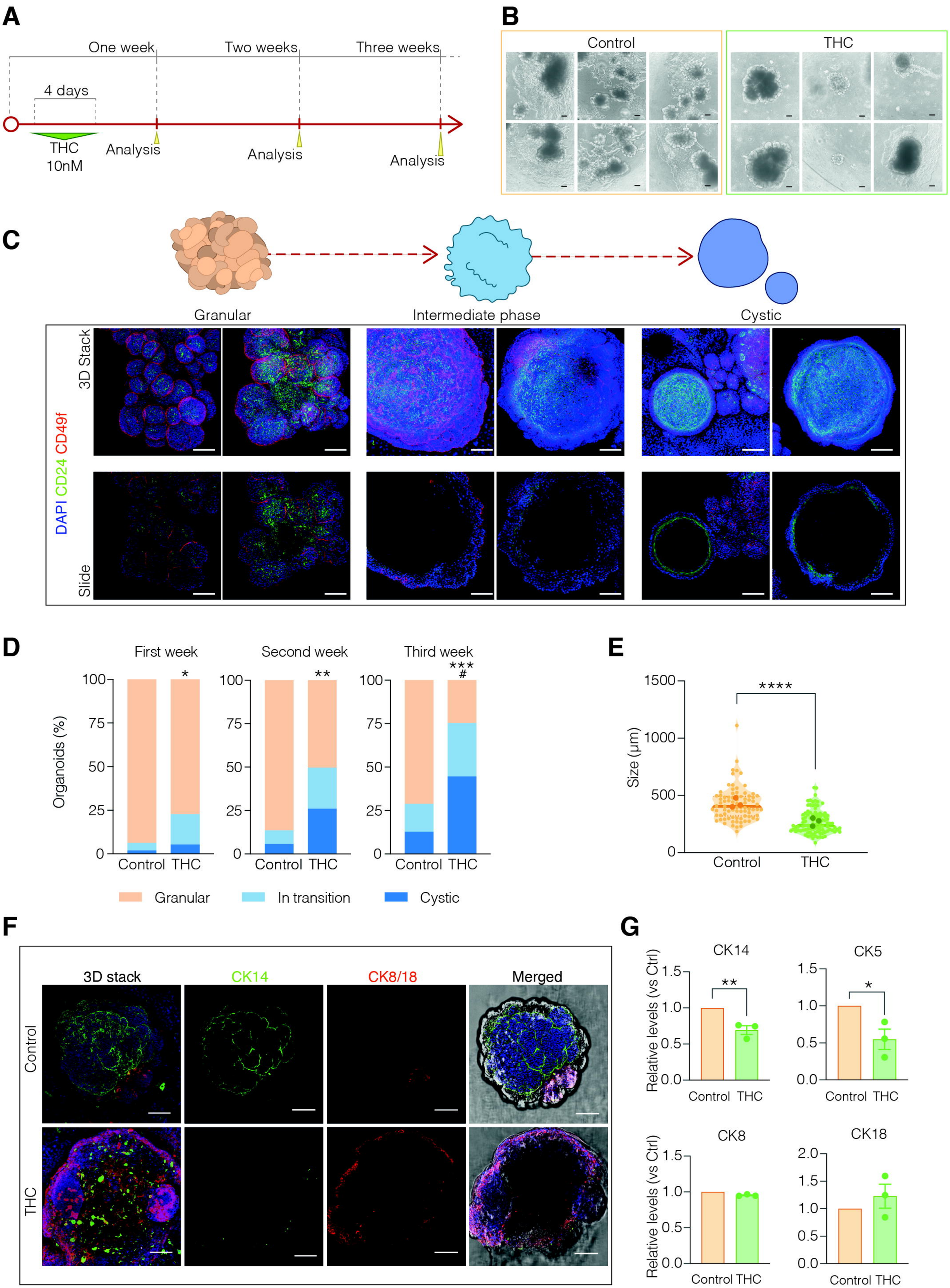
A
One week
Two weeks
Three weeks
4 days
THC
10nM
Analysis
Analysis
Analysis
B
Control
THC
C
Granular
Intermediate phase
Cystic
3D Stack
Slide
DAPI CD24 CD49f
D
First week
Second week
Third week
Organoids (%)
Control THC
Granular
In transition
Cystic
E
Size (µm)
Control
THC
F
3D stack
CK14
CK8/18
Merged
Control
THC
G
CK14
CK5
CK8
CK18
Relative levels (vs Ctrl)
Control THC

Figure 2

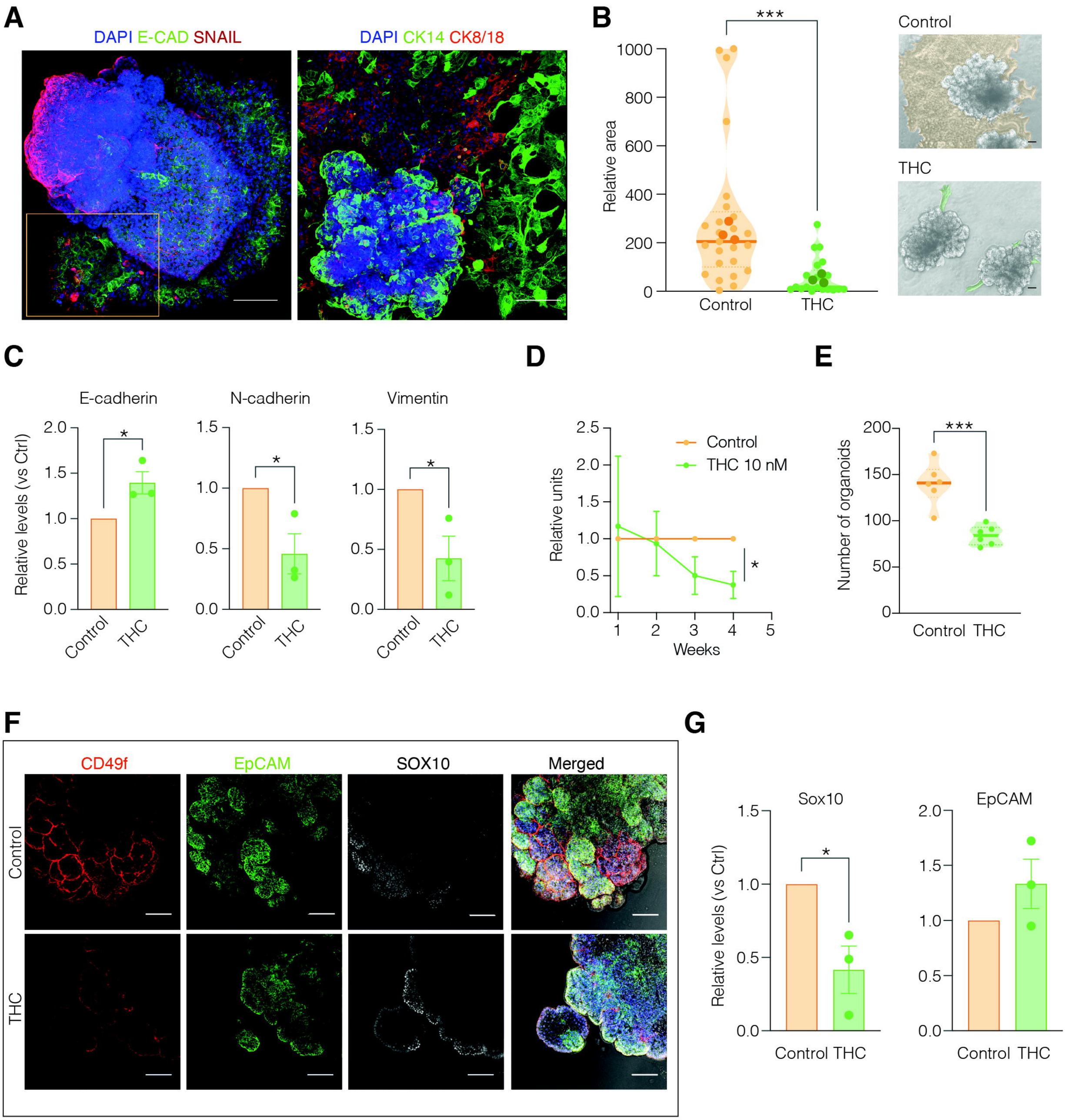
A
DAPI E-CAD SNAIL
DAPI CK14 CK8/18
B
***
Relative area
1000
800
600
400
200
0
Control
THC
Control
THC
C
E-cadherin
N-cadherin
Vimentin
Relative levels (vs Ctrl)
2.0
1.5
1.0
0.5
0.0
*
Control
THC
D
Relative units
Control
THC 10 nM
Weeks
1
2
3
4
5
E
Number of organoids
200
150
100
50
0
***
Control THC
F
CD49f
EpCAM
SOX10
Merged
Control
THC
G
Sox10
EpCAM
Relative levels (vs Ctrl)
Control THC

Figure 3

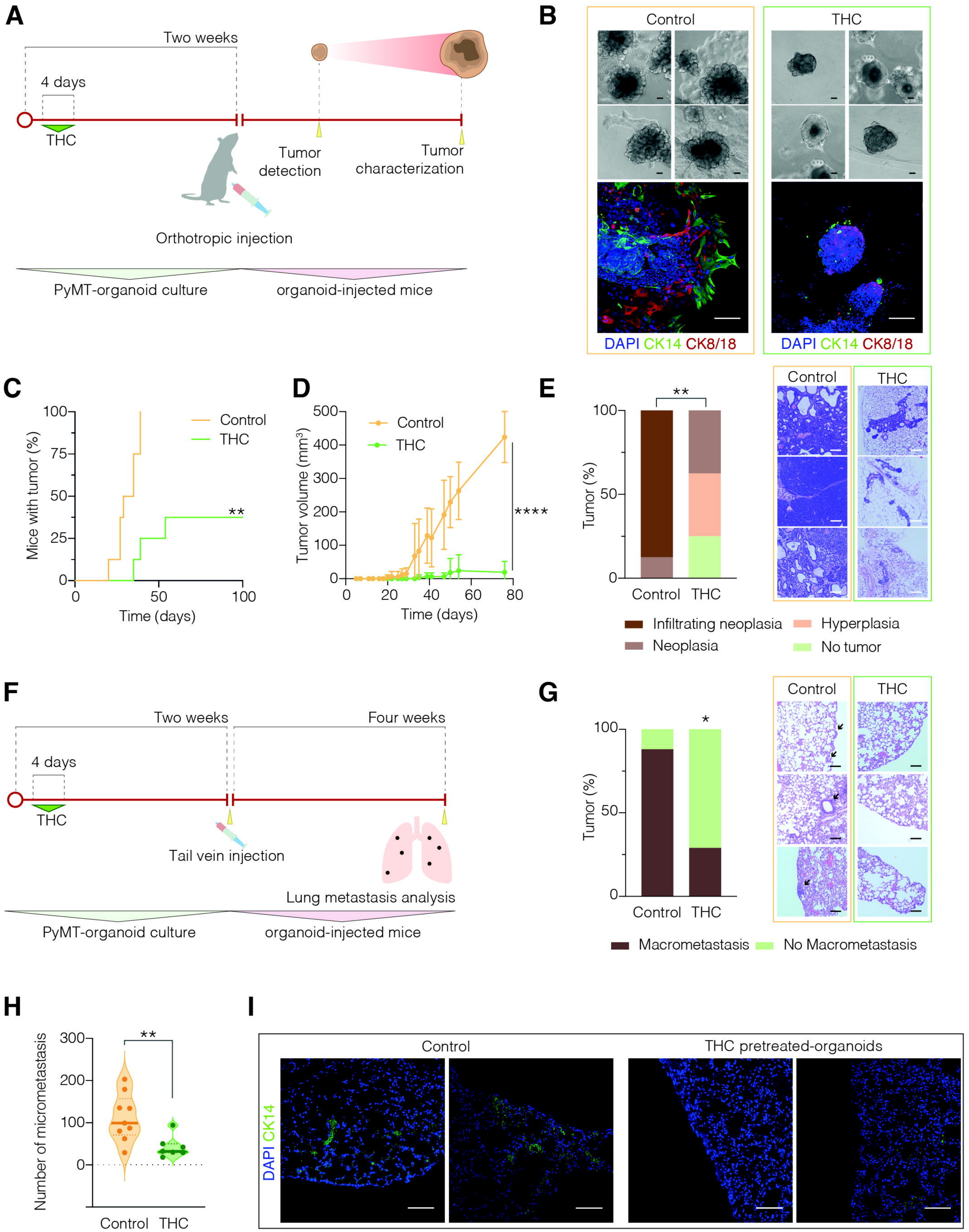
A
Two weeks
4 days
THC
Tumor detection
Tumor characterization
Orthotropic injection
PyMT-organoid culture
organoid-injected mice
B
Control
THC
DAPI CK14 CK8/18
C
Mice with tumor (%)
Control
THC
**
Time (days)
D
Tumor volume (mm³)
Control
THC
****
Time (days)
E
Tumor (%)
**
Control THC
Infiltrating neoplasia
Hyperplasia
Neoplasia
No tumor
F
Two weeks
Four weeks
4 days
THC
Tail vein injection
Lung metastasis analysis
PyMT-organoid culture
organoid-injected mice
G
Tumor (%)
*
Control THC
Macrometastasis
No Macrometastasis
H
Number of micrometastasis
**
Control THC
I
Control
THC pretreated-organoids
DAPI CK14

Figure 4

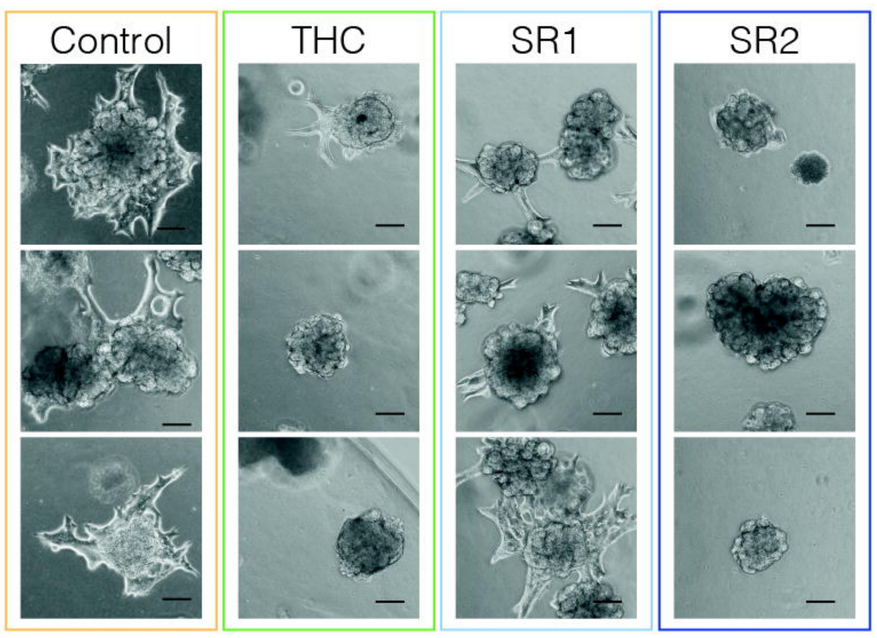
A
Control
THC
SR1
SR2

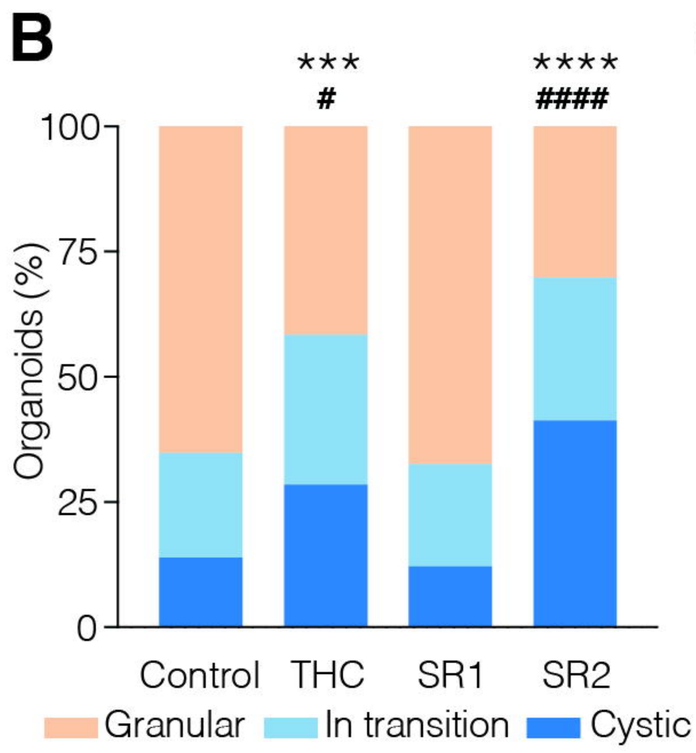
B
***
#
****
####
100
75
50
25
0
Organoids (%)
Control
THC
SR1
SR2
Granular
In transition
Cystic

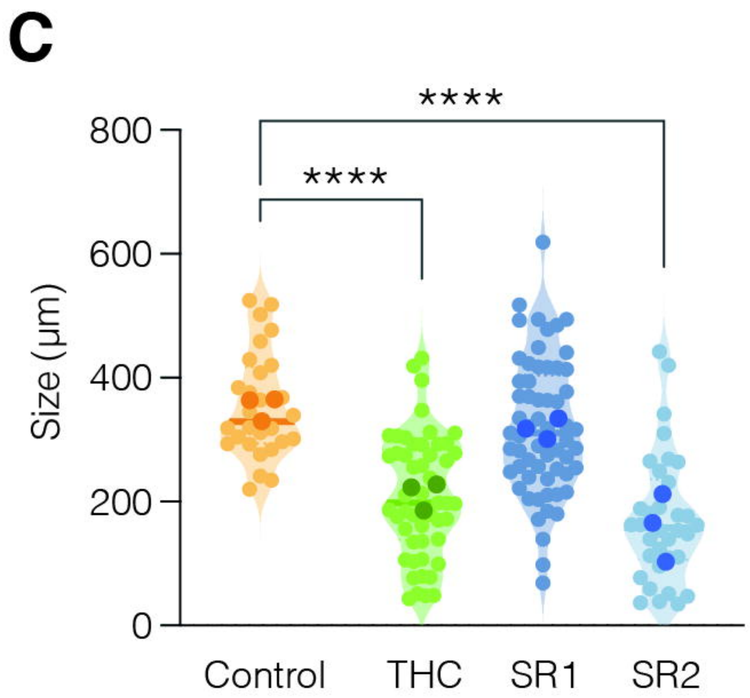
C
****
****
800
600
400
200
0
Size (µm)
Control
THC
SR1
SR2

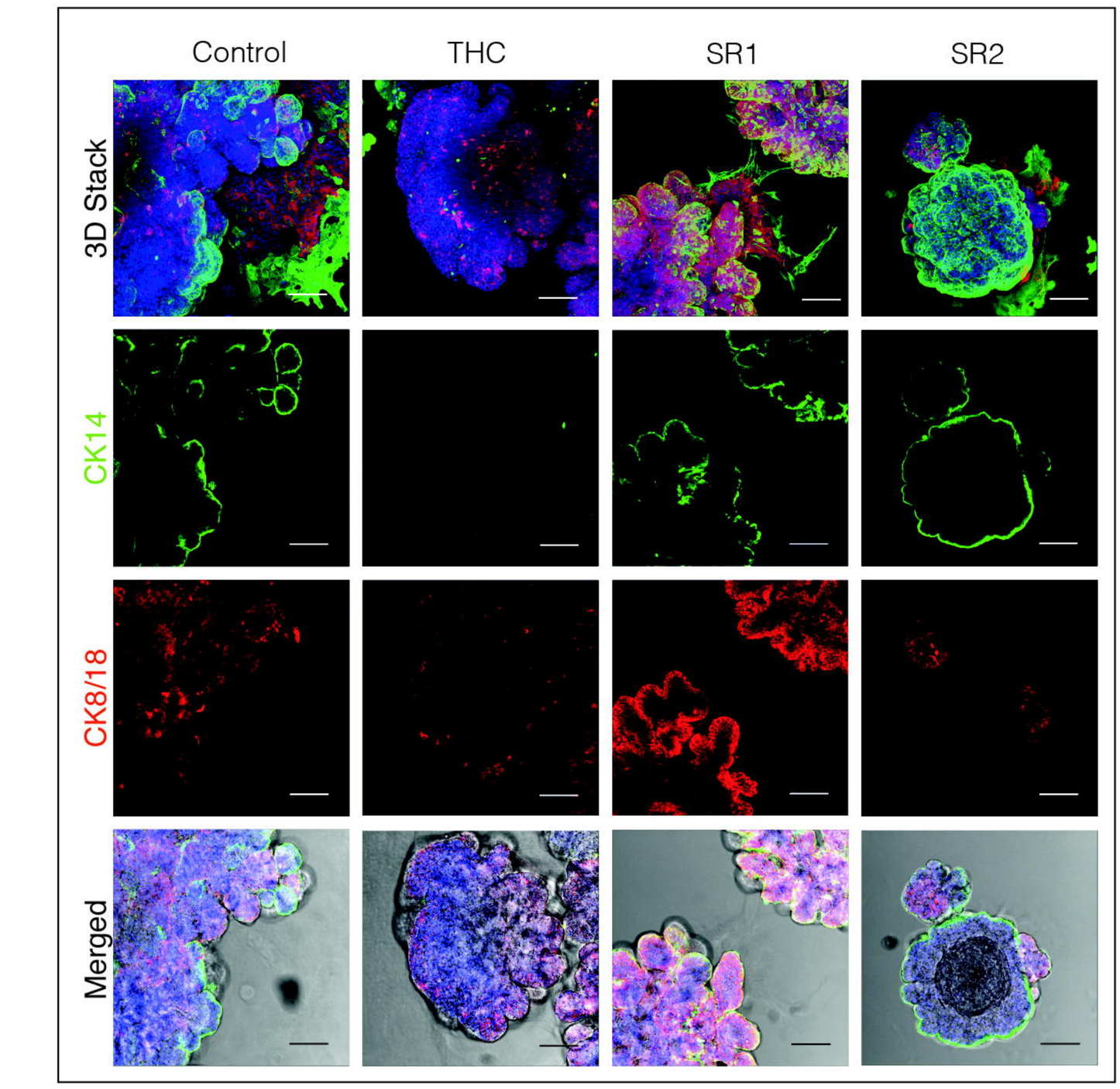
D
Control
THC
SR1
SR2
3D Stack
CK14
CK8/18
Merged

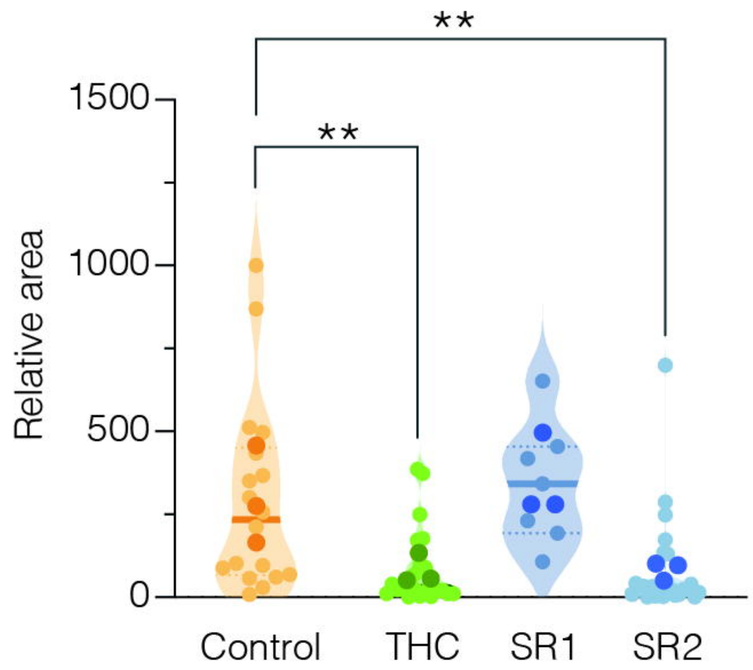
E
**
**
1500
1000
500
0
Relative area
Control
THC
SR1
SR2

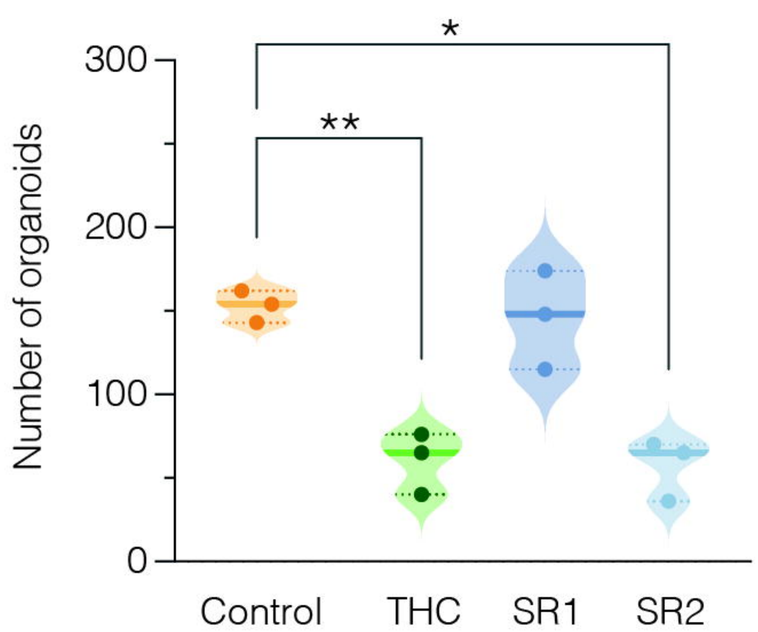
F
*
**
300
200
100
0
Number of organoids
Control
THC
SR1
SR2

Figure 5

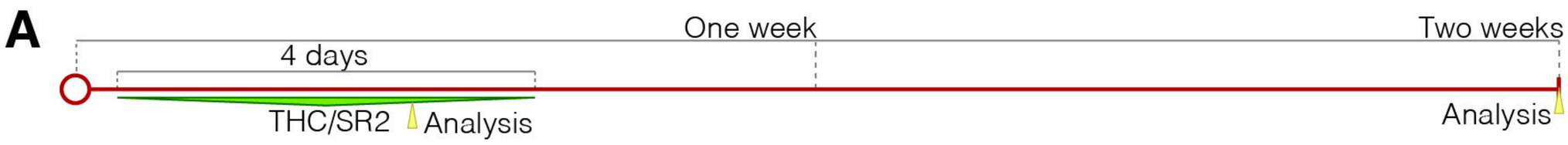

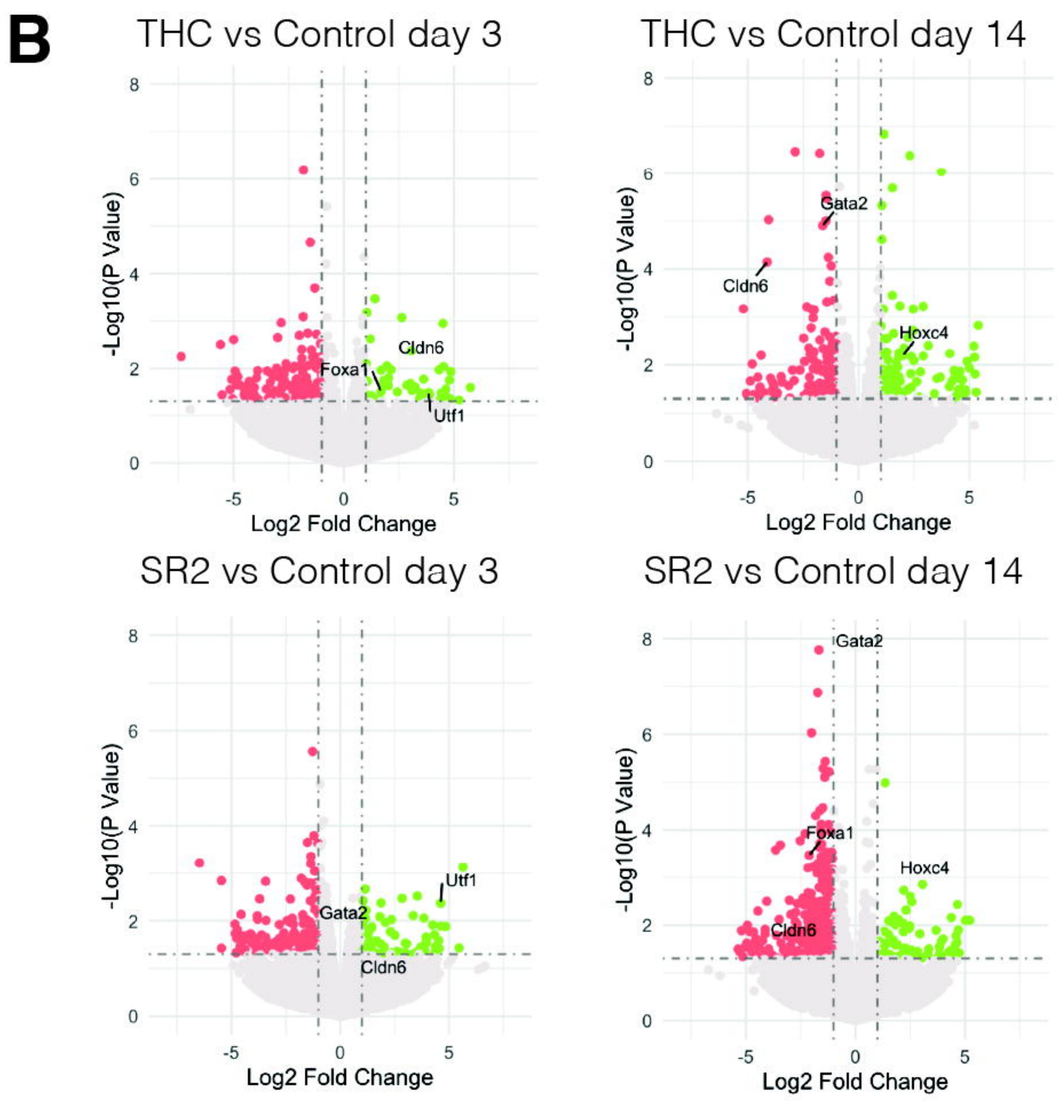

C Control enrichment sets vs SR2

Day 3	NES	Size
N-acetyltransferase activity	-2.00	78
N-acyltransferase activity	-1.89	94
Acetyltransferase activity	-1.81	99
Peptide n-acetyltransferase activity	-1.80	64
Histone exchange	-1.66	16
Histone acetyltransferase activity	-1.54	56
Histone H3K9 modification	-1.53	43
Cromatin silencing	-1.53	60
Histone binding	-1.49	174
Histone H3K9 methylation	-1.49	119
Methylation dependent protein binding	-1.43	62

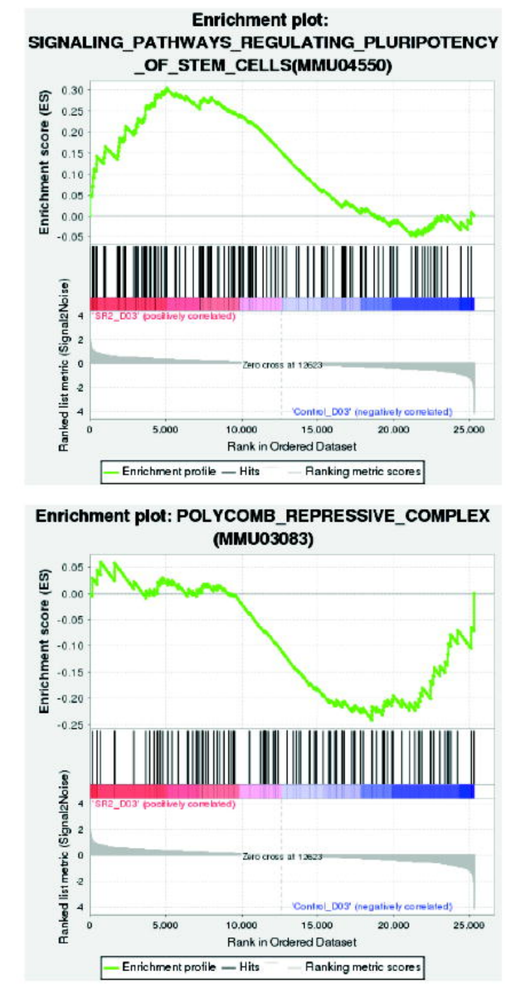

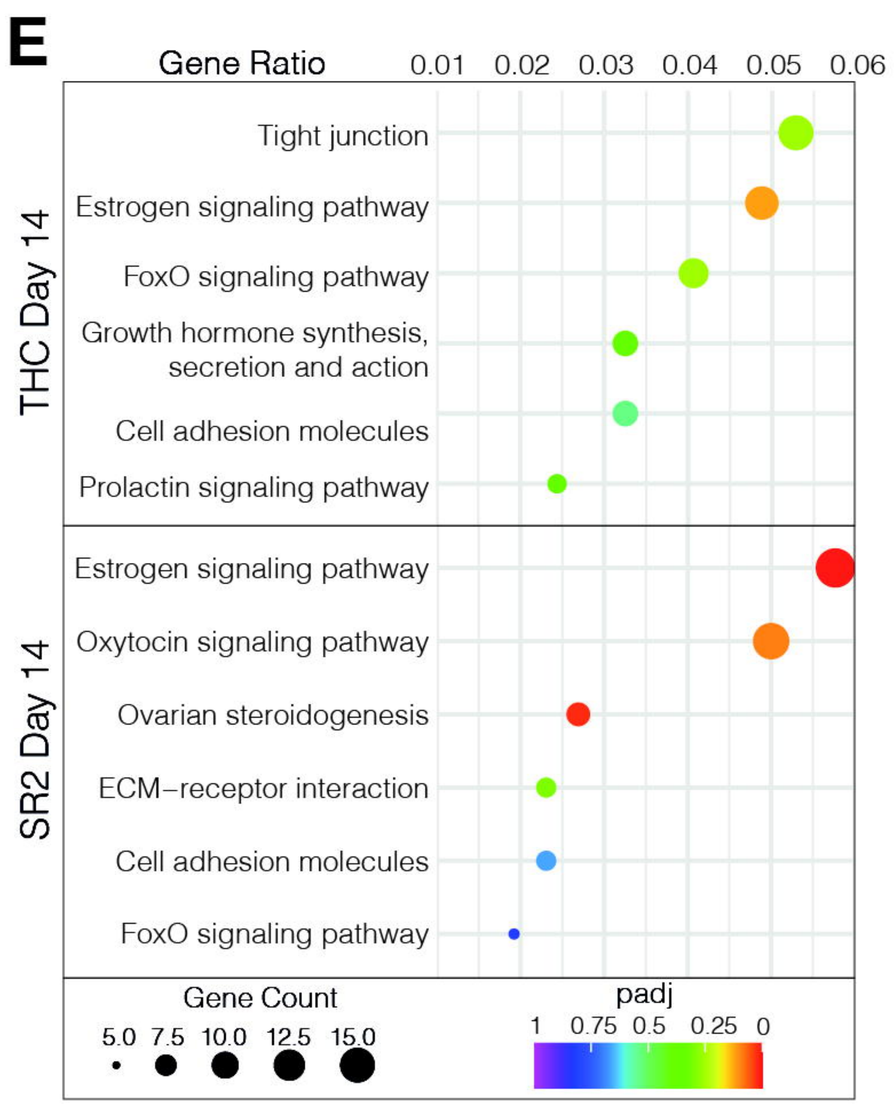

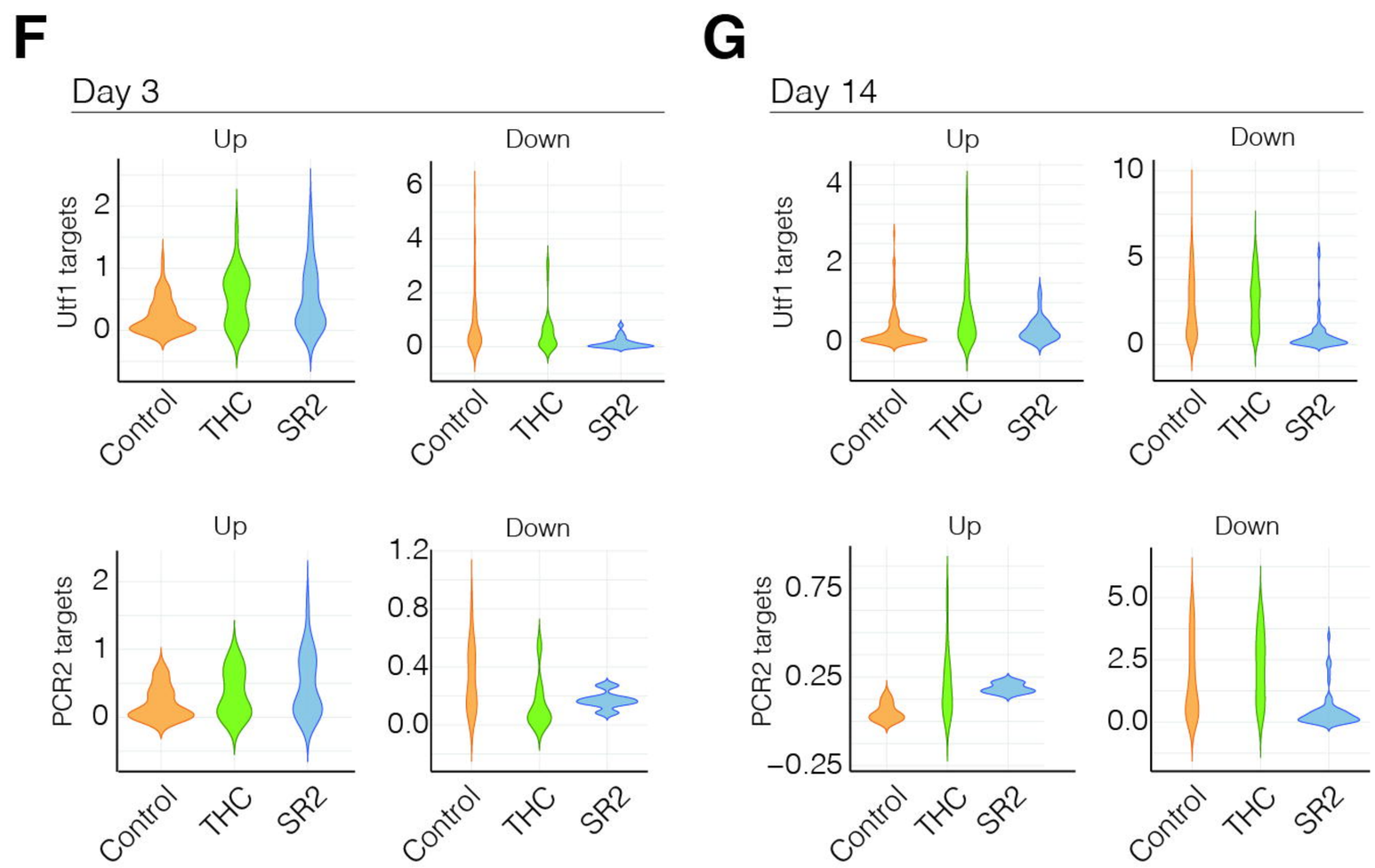

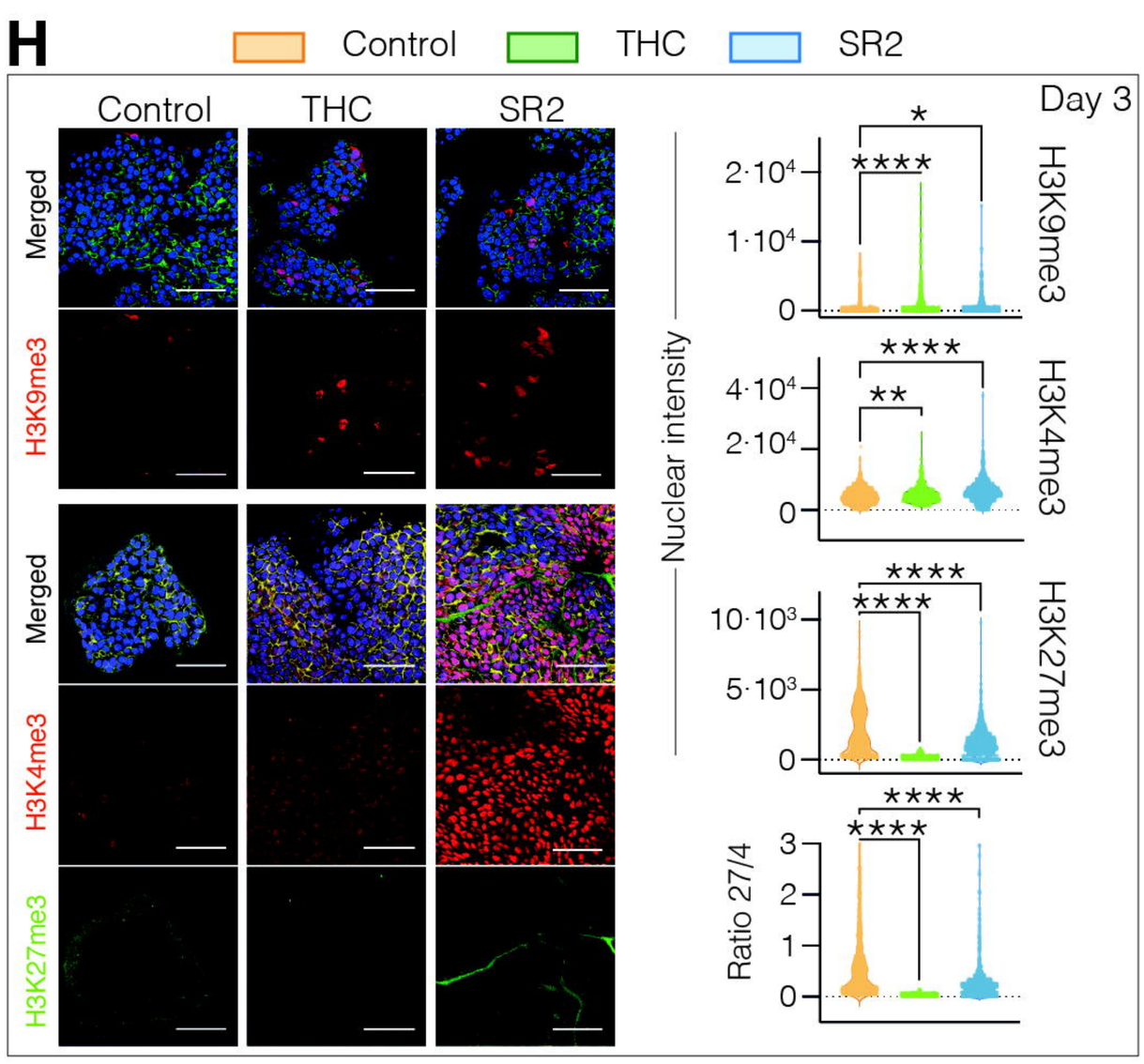

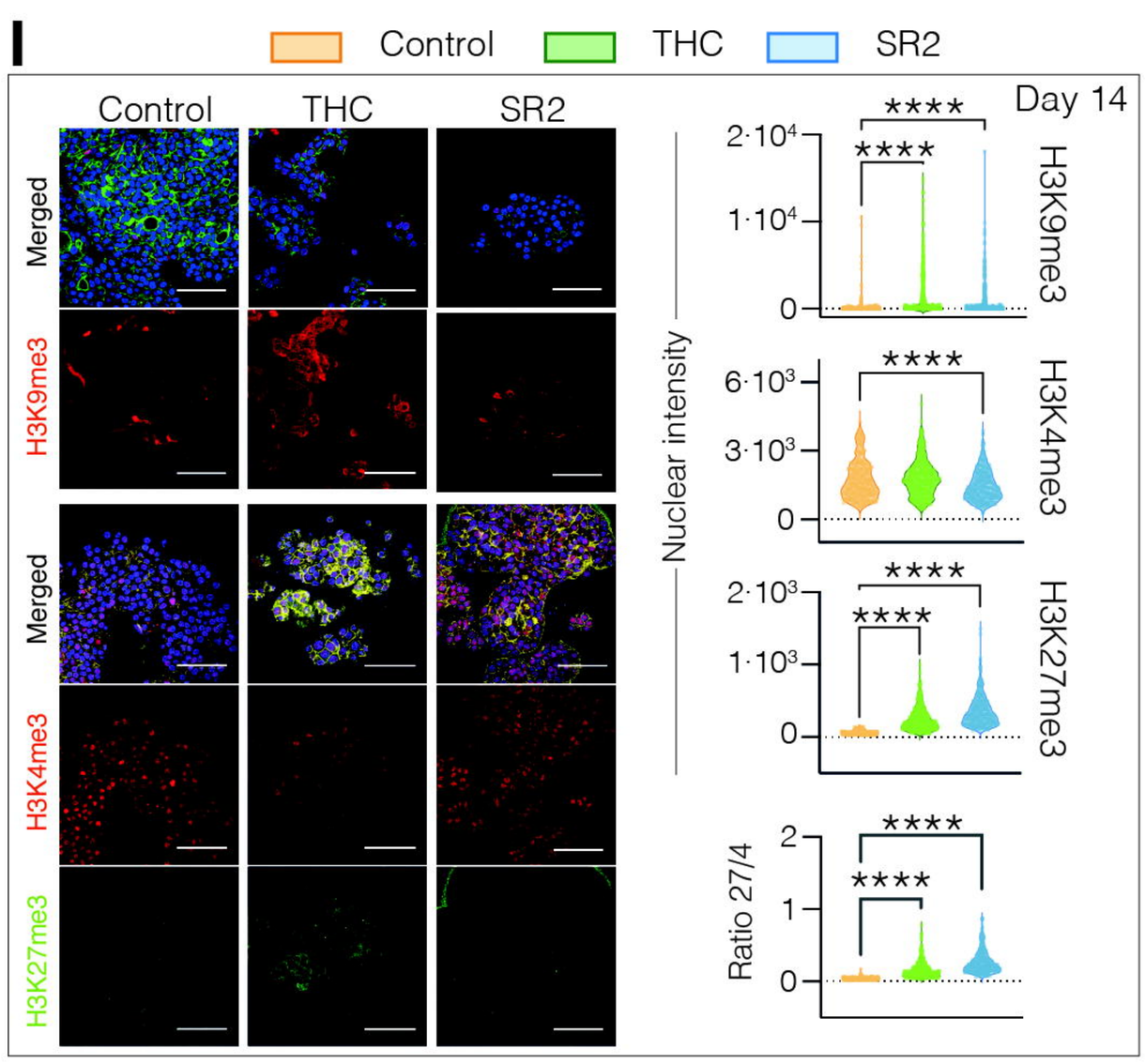

Figure 6

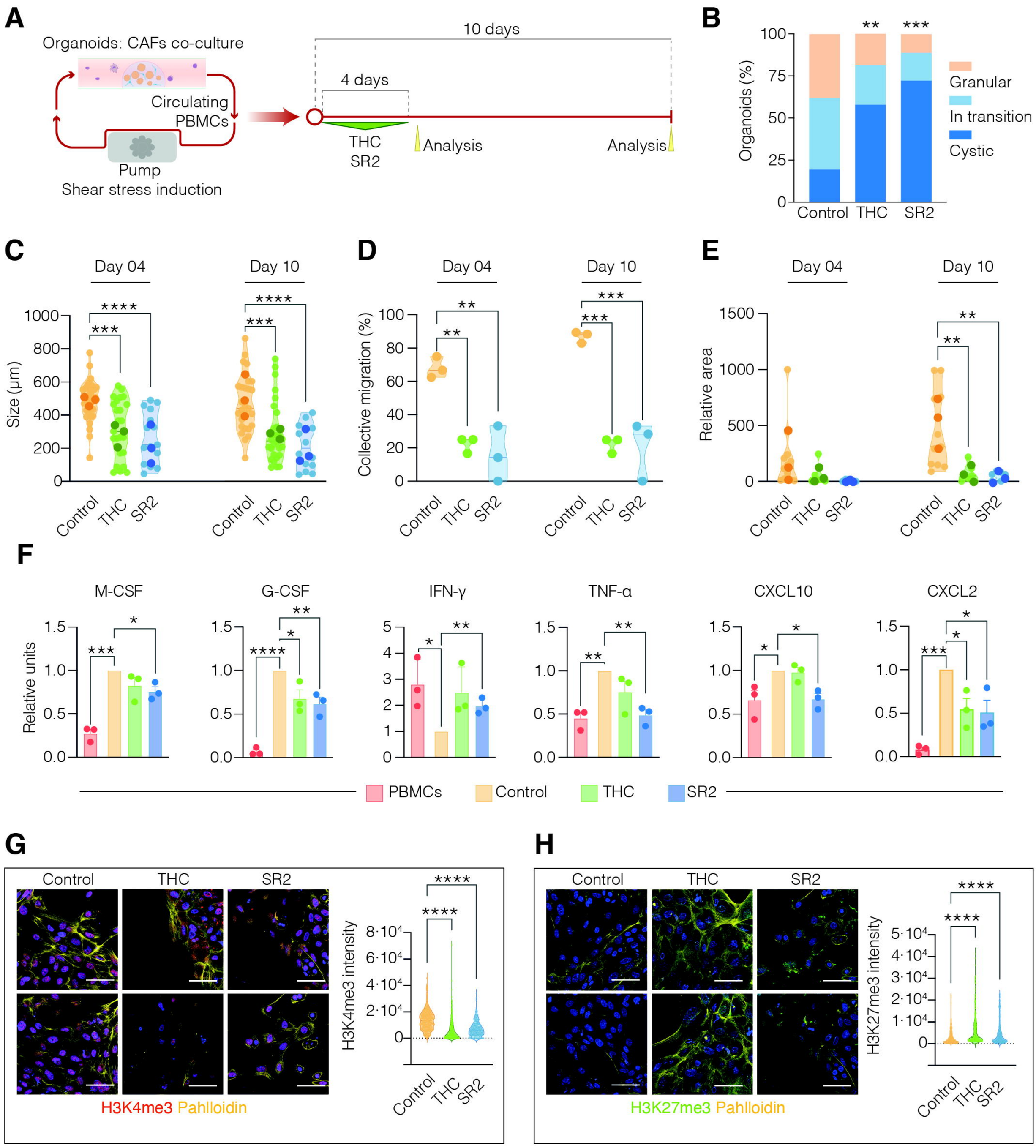
A
Organoids: CAFs co-culture
Circulating PBMCs
Pump
Shear stress induction
10 days
4 days
THC
SR2
Analysis
Analysis
B
Organoids (%)
Granular
In transition
Cystic
Control
THC
SR2
C
Day 04
Day 10
Size (µm)
D
Collective migration (%)
E
Relative area
F
M-CSF
G-CSF
IFN-γ
TNF-α
CXCL10
CXCL2
Relative units
PBMCs
Control
THC
SR2
G
H3K4me3 Pahlloidin
H3K4me3 intensity
H
H3K27me3 Pahlloidin
H3K27me3 intensity

Figure 7

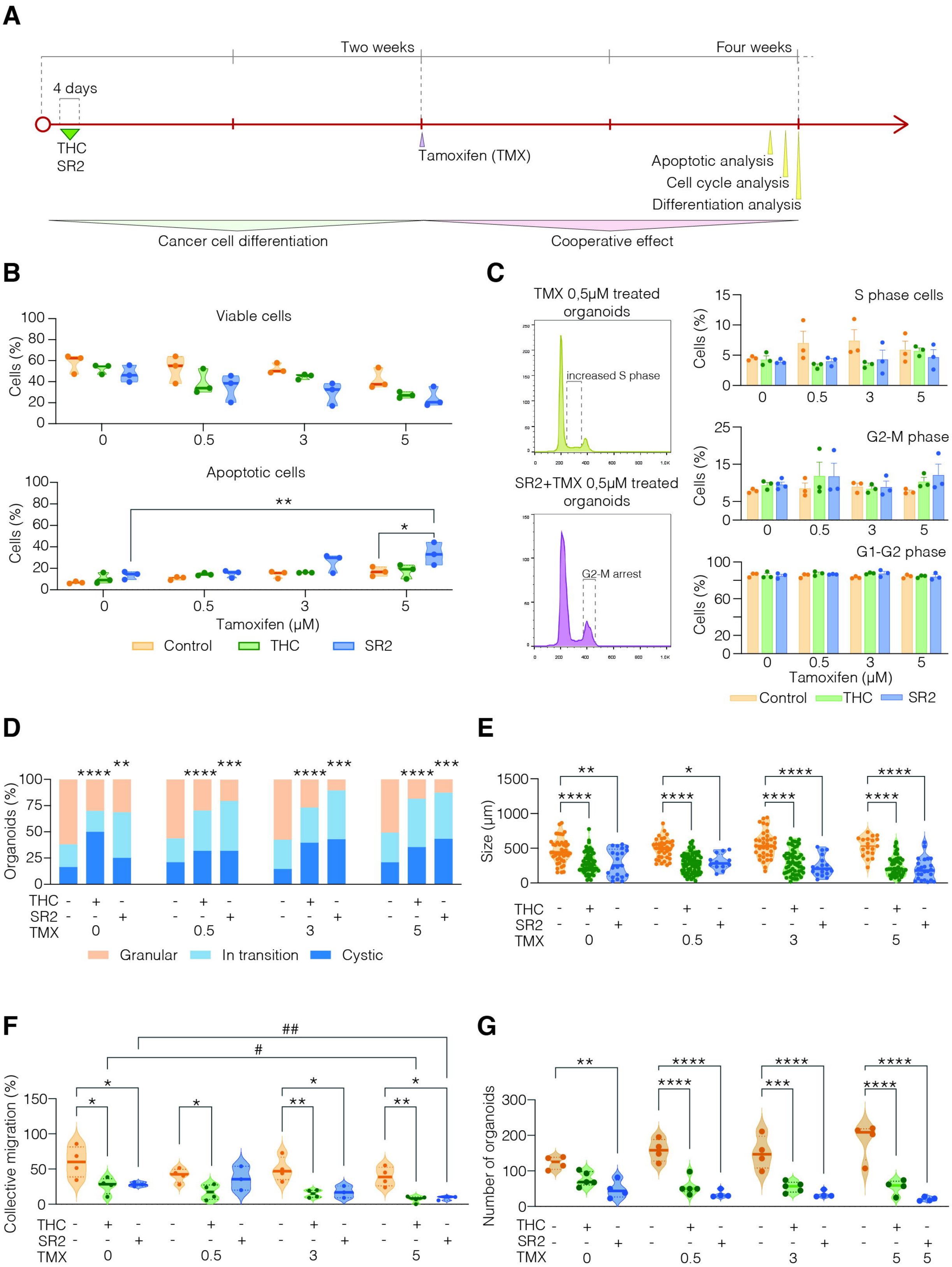
A
Two weeks
Four weeks
4 days
THC
SR2
Tamoxifen (TMX)
Apoptotic analysis
Cell cycle analysis
Differentiation analysis
Cancer cell differentiation
Cooperative effect
B
Viable cells
Cells (%)
Apoptotic cells
Tamoxifen (μM)
Control
THC
SR2
C
TMX 0,5μM treated organoids
increased S phase
SR2+TMX 0,5μM treated organoids
G2-M arrest
S phase cells
G2-M phase
G1-G2 phase
D
Organoids (%)
Granular
In transition
Cystic
E
Size (μm)
F
Collective migration (%)
G
Number of organoids

Figure 8

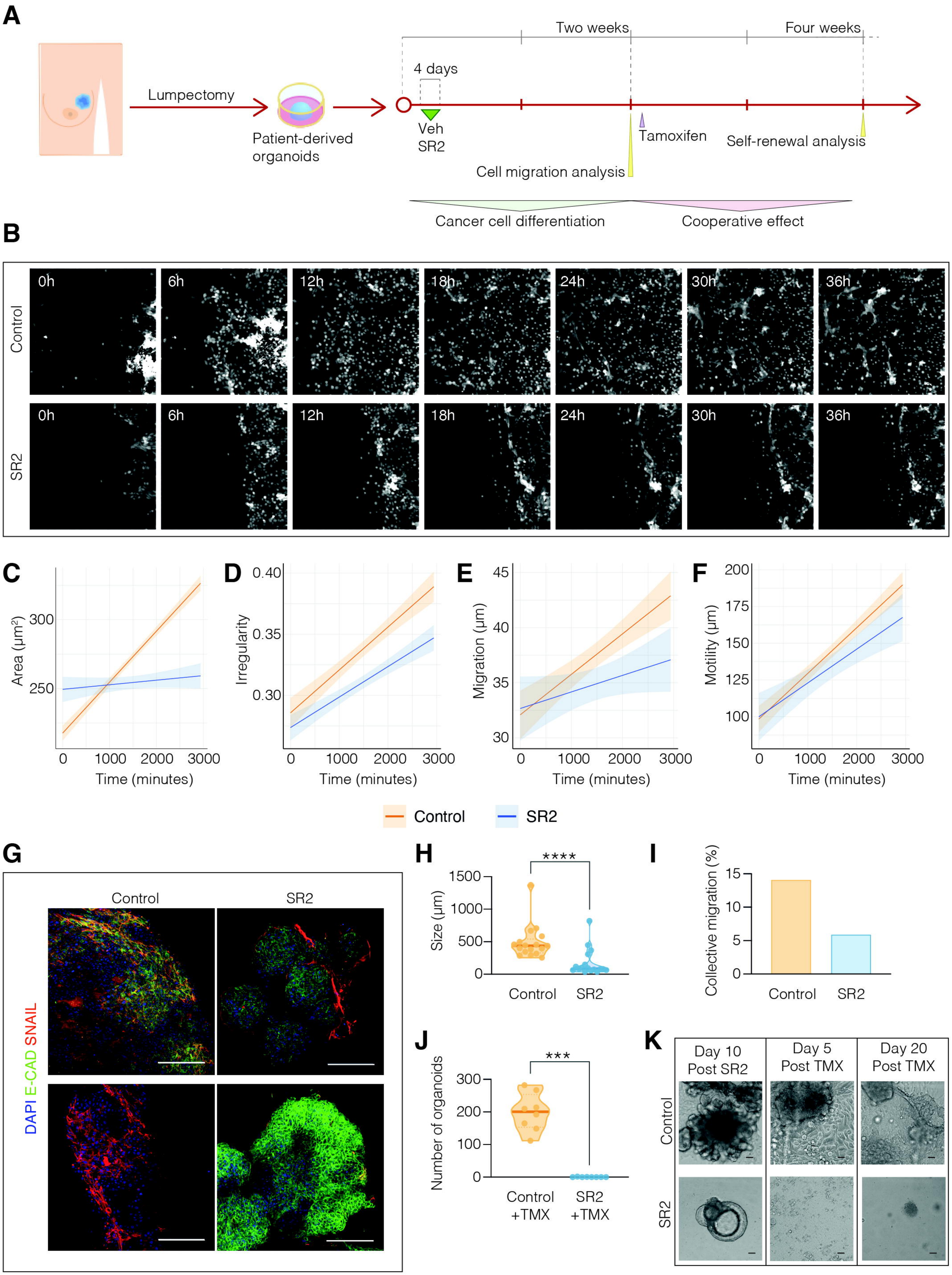
A
Lumpectomy
Patient-derived organoids
4 days
Two weeks
Four weeks
Veh
SR2
Tamoxifen
Self-renewal analysis
Cell migration analysis
Cancer cell differentiation
Cooperative effect
B
Control
SR2
0h
6h
12h
18h
24h
30h
36h
C
Area (µm²)
Time (minutes)
D
Irregularity
Time (minutes)
E
Migration (µm)
Time (minutes)
F
Motility (µm)
Time (minutes)
Control
SR2
G
Control
SR2
DAPI E-CAD SNAIL
H
Size (µm)
****
Control
SR2
I
Collective migration (%)
Control
SR2
J
Number of organoids
***
Control +TMX
SR2 +TMX
K
Day 10 Post SR2
Day 5 Post TMX
Day 20 Post TMX
Control
SR2